# Three-Dimensional Sound Field Reproduction Based on Weighted Mode-Matching Method

Natsuki Ueno, *Student Member, IEEE*, Shoichi Koyama, *Member, IEEE*, and Hiroshi Saruwatari, *Member, IEEE*

***Abstract*—A sound field reproduction method based on the spherical wavefunction expansion of sound fields is proposed, which can be flexibly applied to various array geometries and directivities. First, we formulate sound field synthesis as a minimization problem of some norm on the difference between the desired and synthesized sound fields, and then the optimal driving signals are derived by using the spherical wavefunction expansion of the sound fields. This formulation is closely related to the mode-matching method; a major advantage of the proposed method is the optimal weight on the mode determined according to the norm to be minimized instead of the empirical truncation in the mode-matching method. We also provide some examples of norms and their corresponding weights in analytical forms. Both interior and exterior sound field reproduction are considered in the proposed method, and some applications, such as multizone reproduction and interior reproduction with exterior cancellation, are also discussed. Numerical simulation results indicated that higher reproduction accuracy can be achieved by the proposed method than by the current pressure-matching and mode-matching methods.**

***Index Terms*—Mode-matching method, sound field reproduction, spherical wavefunction expansion.**

## I. Introduction

THE aim of sound field reproduction is to physically synthesize a desired sound field over a target region using multiple loudspeakers. Owing to its potential application to high-fidelity audio systems, it has attracted much attention in the field of spatial-audio research in recent years.

One major approach is an analytic method based on the assumption of a continuous loudspeaker distribution. Furthermore, this approach is classified into two types according to its underlying theory: Kirchhoff–Helmholtz or Rayleigh integrals [1]–[5] (e.g., Wave Field Synthesis) and the spatial Fourier representation of sound fields [6]–[9] (e.g., Spectral Division Method). In these methods, the desired sound field is reproduced over the entire space enclosed by the loudspeaker array or over the half space bounded by a planar array in the case of Wave Field Synthesis. However, these methods basically require a simple array geometry such as a line, plane, circle, or sphere, which obviously limits their scope of practical application.

Several methods such as the pressure-matching method [10]–[12] and mode-matching method [3], [13]–[15] can be more flexibly applied to various array configurations and directivities. The pressure-matching method is formulated so that the synthesized sound pressures correspond to the desired ones at the given discrete control points, and the driving signals are usually obtained by the least-squares method with regularization. Owing to its simple formulation, this method can be applied in almost any situation; however, inevitable errors occur away from the control points, especially in cases when the control points are coarsely arranged. Although this problem can be prevented to some extent by finely arranging the control points over the target region, the computational cost also increases with the number of control points. On the other hand, the mode-matching method aims to match the modes of the synthesized and desired sound fields at a certain control point, which is often used in Higher-Order Ambisonics approach. A "mode" in the three-dimensional (3D) context usually means a spherical wavefunction, by which a sound field can be expanded, and the expansion coefficient is also called an ambisonic component or coefficient in the literature of Higher-Order Ambisonics [16]. Since the spherical wavefunctions, which are the products of spherical Bessel functions and spherical harmonics, are the solutions of the Helmholtz equation, the mode-matching method exploits its constraint. This is a major difference between the mode-matching method and the pressure-matching method. However, it is necessary in the mode-matching method to truncate the modes in an empirical manner, which strongly affects its reproduction accuracy. Note that an excessively large or small truncation order leads to performance degradation in the mode-matching method.

For the two-dimensional (2D) case, Betlehem and Abhayapala [15] proposed the weighting of expansion coefficients in the mode-matching method to minimize the spatial reproduction error in the context of reverberant sound field control. Our previous works [17]–[19] addressed the weights of expansion coefficients, and their advantage over the empirical truncation in the mode-matching method was shown for the 2D case. Since the optimal weightings on the expansion coefficients are analytically derived according to the objective function to be minimized (e.g., the spatial squared error of the sound pressure inside the given target region), these methods can be referred to as *weighted mode-matching methods*. Only specific cases in the 2D space

Manuscript received October 26, 2018; revised May 30, 2019; accepted July 28, 2019. Date of publication August 14, 2019; date of current version August 26, 2019. This work was supported in part by JSPS KAKENHI under Grants JP15H05312, JP16H01735, and JP18J21926, and in part by the SECOM Science and Technology Foundation. The Associate Editor coordinating the review of this manuscript and approving it for publication was Dr. Huseyin Hacihabiboglu. *(Corresponding author: Natsuki Ueno.)*

The authors are with the Graduate School of Information Science and Technology, University of Tokyo, Tokyo 113-8656, Japan (e-mail: natsuki_ueno@ipc.i.u-tokyo.ac.jp; koyama.shoichi@ieee.org; hiroshi_saruwatari@ipc.i.u-tokyo.ac.jp).

Digital Object Identifier 10.1109/TASLP.2019.2934834

2329-9290 © 2019 IEEE. Personal use is permitted, but republication/redistribution requires IEEE permission.
See http://www.ieee.org/publications_standards/publications/rights/index.html for more information.

were considered in these works; therefore, more general cases in the 3D space have to be investigated.

In this study, our goal is twofold: to establish the general concept of the weighted mode-matching method in the 3D space and to propose several examples of weights that are derived in analytical forms. We consider both interior and exterior sound field reproduction, where sound fields are expanded by the interior and exterior spherical wavefunctions, respectively.

The rest of this paper is organized as follows. In Section II, we introduce several notations and basic theories on the spherical wavefunction expansion of sound fields, which are used throughout this paper. In Section III, two current methods, the pressure-matching method and the mode-matching method, are briefly introduced. In Section IV, we describe the proposed method, where both the general concept of the weighted mode-matching method and several examples of the norms and corresponding weights are given. We also discuss some possible applications such as multizone reproduction [20]–[22] and interior reproduction with exterior cancellation [5], [13], [19]. In Section V, several numerical experiments performed to evaluate the proposed method are described and their results are given. Finally, we present our conclusions in Section VI.

## II. Notations and Preliminaries

First, we introduce several notations and basic theories used throughout this paper.

### A. Notations

Suppose that $L$ secondary sources, i.e., loudspeakers, are located at $\boldsymbol{r}_1, \ldots, \boldsymbol{r}_L$ with an arbitrary geometry in the 3D space $\mathbb{R}^3$. The $l$th loudspeaker's driving signal at (angular) frequency $\omega$ is denoted by $d_l(\omega)$, and the vector of the driving signals is denoted by $\boldsymbol{d}(\omega) = [d_1(\omega), \ldots, d_L(\omega)]^{\mathsf{T}}$, where the superscript $\mathsf{T}$ denotes the transpose. Similarly, the $l$th loudspeaker's transfer function at position $\boldsymbol{r}$ and frequency $\omega$ is denoted by $g_l(\boldsymbol{r}, \omega)$. Then, the synthesized sound pressure $u_{\mathrm{syn}}(\boldsymbol{r}, \omega)$ is represented as

$$u_{\mathrm{syn}}(\boldsymbol{r}, \omega) = \sum_{l=1}^{L} d_l(\omega) g_l(\boldsymbol{r}, \omega). \tag{1}$$

Hereafter, we omit $\omega$ for notational simplicity. In addition, we refer to the function $u_{\mathrm{syn}}$ as the synthesized sound field, and we also use the same notation for all other sound fields.

We address two sound field reproduction problems: interior sound field reproduction and exterior sound field reproduction. Let $S_{\mathrm{int}}$ be a spherical surface centered at $\boldsymbol{r}_{\mathrm{c}}$ not including any secondary sources and $S_{\mathrm{ext}}$ be a spherical surface centered at $\boldsymbol{r}_{\mathrm{c}}$ including all the secondary sources as shown in Fig. 1. We define $\Omega_{\mathrm{int}}$ as a region inside $S_{\mathrm{int}}$ and $\Omega_{\mathrm{ext}}$ as a region outside $S_{\mathrm{ext}}$. An interior sound field is defined as a sound field such that the sound sources exist only outside $S_{\mathrm{int}}$, and an exterior sound field is defined as a sound field such that the sound sources exist only inside $S_{\mathrm{ext}}$. The objective of interior sound field reproduction is to reproduce a given desired interior sound field inside $S_{\mathrm{int}}$, and that of exterior sound field reproduction is to reproduce a given desired exterior sound field outside $S_{\mathrm{ext}}$. In either case, the desired sound field is denoted by $u_{\mathrm{des}}$.

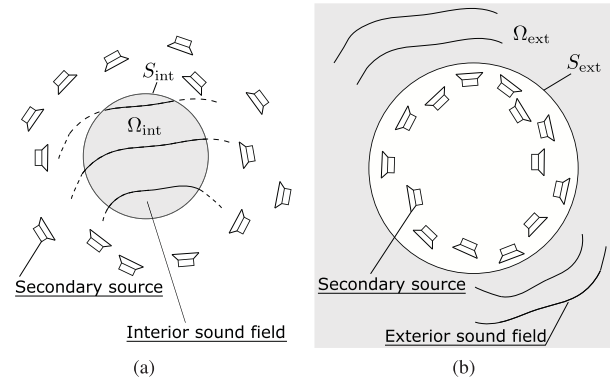


Fig. 1. Settings of secondary sources and target region. (a) Interior sound field reproduction; (b) exterior sound field reproduction.

### B. Spherical Wavefunction Expansion of Interior Sound Fields

In the case of interior sound field reproduction, $g_l$ and $u_{\mathrm{des}}$ can be expanded at the expansion center $\boldsymbol{r}_{\mathrm{c}}$ as [23]

$$u_{\mathrm{des}}(\boldsymbol{r}) = \sum_{\nu,\mu} \mathring{u}^{\mathrm{int}}_{\mathrm{des},\nu,\mu}(\boldsymbol{r}_{\mathrm{c}}) \varphi_{\nu,\mu}(\boldsymbol{r} - \boldsymbol{r}_{\mathrm{c}}), \tag{2}$$

$$g_l(\boldsymbol{r}) = \sum_{\nu,\mu} \mathring{g}^{\mathrm{int}}_{l,\nu,\mu}(\boldsymbol{r}_{\mathrm{c}}) \varphi_{\nu,\mu}(\boldsymbol{r} - \boldsymbol{r}_{\mathrm{c}}), \tag{3}$$

where $\sum_{\nu,\mu}$ is the abbreviated form of $\sum_{\nu=0}^{\infty} \sum_{\mu=-\nu}^{\nu}$. In (2) and (3), $\mathring{u}^{\mathrm{int}}_{\mathrm{des},\nu,\mu}(\boldsymbol{r}_{\mathrm{c}})$ and $\mathring{g}^{\mathrm{int}}_{l,\nu,\mu}(\boldsymbol{r}_{\mathrm{c}})$ are the interior expansion coefficients at the expansion center $\boldsymbol{r}_{\mathrm{c}}$, and $\varphi_{\nu,\mu}(\cdot)$ is the interior spherical wavefunction defined as

$$\varphi_{\nu,\mu}(\boldsymbol{r}) = \sqrt{4\pi} j_\nu(kr) Y_{\nu,\mu}(\hat{\boldsymbol{r}}), \tag{4}$$

where $k = \omega/c$ is the wavenumber at the sound speed $c$, $j_\nu(\cdot)$ is the $\nu$th-order spherical Bessel function of the first kind [24], $Y_{\nu,\mu}(\cdot)$ is the spherical harmonic function of order $\nu$ and degree $\mu$ [24], and $r$ and $\hat{\boldsymbol{r}}$ are defined respectively as $r = \|\boldsymbol{r}\|$ and $\hat{\boldsymbol{r}} = \boldsymbol{r}/r$ with the Euclidean norm $\|\cdot\|$.

The interior expansion coefficients of the transfer functions and the desired sound field can be obtained in several ways. If they are modeled or represented analytically (e.g., by multipoles or plane waves), their interior expansion coefficients can be calculated using several mathematical formulae [3], [24]. Another approach is to directly measure the interior expansion coefficients by using a microphone array [3], [25]–[31]. Hereafter, $\mathring{u}^{\mathrm{int}}_{\mathrm{des},\nu,\mu}(\boldsymbol{r}_{\mathrm{c}})$ and $\mathring{g}^{\mathrm{int}}_{l,\nu,\mu}(\boldsymbol{r}_{\mathrm{c}})$ are assumed to be given.

### C. Spherical Wavefunction Expansion of Exterior Sound Fields

In the case of exterior sound field reproduction, $g_l$ and $u_{\mathrm{des}}$ can be expanded at the expansion center $\boldsymbol{r}_{\mathrm{c}}$ as [23], [32]

$$u_{\mathrm{des}}(\boldsymbol{r}) = \sum_{\nu,\mu} \mathring{u}^{\mathrm{ext}}_{\mathrm{des},\nu,\mu}(\boldsymbol{r}_{\mathrm{c}}) \psi_{\nu,\mu}(\boldsymbol{r} - \boldsymbol{r}_{\mathrm{c}}), \tag{5}$$

$$g_l(\boldsymbol{r}) = \sum_{\nu,\mu} \mathring{g}^{\mathrm{ext}}_{l,\nu,\mu}(\boldsymbol{r}_{\mathrm{c}}) \psi_{\nu,\mu}(\boldsymbol{r} - \boldsymbol{r}_{\mathrm{c}}). \tag{6}$$

In (5) and (6), $\mathring{u}^{\mathrm{ext}}_{\mathrm{des},\nu,\mu}(\boldsymbol{r}_{\mathrm{c}})$ and $\mathring{g}^{\mathrm{ext}}_{l,\nu,\mu}(\boldsymbol{r}_{\mathrm{c}})$ are the exterior expansion coefficients at the expansion center $\boldsymbol{r}_{\mathrm{c}}$, and $\psi_{\nu,\mu}(\cdot)$ is the exterior spherical wavefunction defined as

$$\psi_{\nu,\mu}(\boldsymbol{r}) = \sqrt{4\pi} h_{\nu}(kr) Y_{\nu,\mu}(\hat{\boldsymbol{r}}), \tag{7}$$

where $h_{\nu}(\cdot)$ is the $\nu$th-order spherical Hankel function of the first kind [24].

Similarly to the interior expansion coefficients, these exterior expansion coefficients can be derived analytically using mathematical formulae [24] or measured by using a microphone array [29], [30]. Hereafter, $\mathring{u}^{\mathrm{ext}}_{\mathrm{des},\nu,\mu}(\boldsymbol{r}_{\mathrm{c}})$ and $\mathring{g}^{\mathrm{ext}}_{l,\nu,\mu}(\boldsymbol{r}_{\mathrm{c}})$ are assumed to be given.

### D. Translation of Expansion Coefficients

When the exterior sound field $u$ is expanded at the expansion center $\boldsymbol{r}_{\mathrm{c}}$ as

$$u(\boldsymbol{r}) = \sum_{\nu,\mu} \mathring{u}^{\mathrm{ext}}_{\nu,\mu}(\boldsymbol{r}_{\mathrm{c}}) \psi_{\nu,\mu}(\boldsymbol{r} - \boldsymbol{r}_{\mathrm{c}}), \tag{8}$$

the expansion coefficients at a different expansion center $\boldsymbol{r}'_{\mathrm{c}}$ are given by the following equations [24]:

$$\mathring{u}^{\mathrm{ext}}_{\nu,\mu}(\boldsymbol{r}'_{\mathrm{c}}) = \sum_{\nu',\mu'} T^{\nu',\mu'}_{\nu,\mu}(\boldsymbol{r}'_{\mathrm{c}} - \boldsymbol{r}_{\mathrm{c}}) \mathring{u}^{\mathrm{ext}}_{\nu',\mu'}(\boldsymbol{r}_{\mathrm{c}}), \tag{9}$$

$$\mathring{u}^{\mathrm{int}}_{\nu,\mu}(\boldsymbol{r}'_{\mathrm{c}}) = \sum_{\nu',\mu'} S^{\nu',\mu'}_{\nu,\mu}(\boldsymbol{r}'_{\mathrm{c}} - \boldsymbol{r}_{\mathrm{c}}) \mathring{u}^{\mathrm{ext}}_{\nu',\mu'}(\boldsymbol{r}_{\mathrm{c}}), \tag{10}$$

where $T^{\nu',\mu'}_{\nu,\mu}(\cdot)$ and $S^{\nu',\mu'}_{\nu,\mu}(\cdot)$ are the translation operators defined as

$$T^{\nu',\mu'}_{\nu,\mu}(\boldsymbol{r}) = 4\pi(-1)^{\mu'} \mathrm{j}^{\nu-\nu'} \cdot \sum_{s=0}^{\nu+\nu'} \mathrm{j}^{s} j_{s}(kr) Y_{s,\mu-\mu'}(\hat{\boldsymbol{r}})^{*} \mathcal{G}(\nu',\mu';\nu,-\mu;s), \tag{11}$$

$$S^{\nu',\mu'}_{\nu,\mu}(\boldsymbol{r}) = 4\pi(-1)^{\mu'} \mathrm{j}^{\nu-\nu'} \cdot \sum_{s=0}^{\nu+\nu'} \mathrm{j}^{s} h_{s}(kr) Y_{s,\mu-\mu'}(\hat{\boldsymbol{r}})^{*} \mathcal{G}(\nu',\mu';\nu,-\mu;s). \tag{12}$$

Here, j is the imaginary unit, the superscript $*$ denotes the complex conjugate, and $\mathcal{G}(\cdot)$ is the Gaunt coefficient [24].

## III. Current Methods

We briefly introduce two current methods that are closely related to the proposed method.

### A. Pressure-Matching Method

The pressure-matching method aims to control the sound pressures at given discrete control points so that they correspond to the desired ones. Regardless of the reproduction of interior or exterior sound fields, a typical formulation is as follows [11]. Let $\boldsymbol{r}^{(1)}_{cp}, \ldots, \boldsymbol{r}^{(M)}_{cp}$ be the positions of the control points. Then, the driving signals are derived by solving the following minimization problem:

$$\underset{\boldsymbol{d}\in\mathbb{C}^{L}}{\mathrm{minimize}} \quad \sum_{m=1}^{M} \left| u_{\mathrm{syn}}(\boldsymbol{r}^{(m)}_{\mathrm{cp}}) - u_{\mathrm{des}}(\boldsymbol{r}^{(m)}_{\mathrm{cp}}) \right|^{2} + \lambda \boldsymbol{d}^{\mathsf{H}} \boldsymbol{d}, \tag{13}$$

where $\lambda$ is the regularization parameter and the superscript $\mathsf{H}$ denotes the Hermitian transpose. As derived in [11], the solution of (13) is given by

$$\hat{\boldsymbol{d}}_{\mathrm{pm}} = (\mathbf{A}_{\mathrm{pm}} + \lambda \boldsymbol{I}_{L})^{-1} \mathbf{b}_{\mathrm{pm}}, \tag{14}$$

where $\boldsymbol{I}_{L}$ is the $L \times L$ identity matrix, and $\mathbf{A}_{\mathrm{pm}} \in \mathbb{C}^{L\times L}$ and $\mathbf{b}_{\mathrm{pm}} \in \mathbb{C}^{L}$ are defined as

$$(\mathbf{A}_{\mathrm{pm}})_{l_1,l_2} = \sum_{m=1}^{M} g_{l_1}(\boldsymbol{r}^{(m)}_{cp})^{*} g_{l_2}(\boldsymbol{r}^{(m)}_{cp}), \tag{15}$$

$$(\mathbf{b}_{\mathrm{pm}})_{l} = \sum_{m=1}^{M} g_{l}(\boldsymbol{r}^{(m)}_{cp})^{*} u_{\mathrm{des}}(\boldsymbol{r}^{(m)}_{cp}). \tag{16}$$

Here, $(\cdot)_{l_1,l_2}$ denotes the $(l_1, l_2)$th element of the matrix and $(\cdot)_{l}$ denotes the $l$th element of the vector.

In many practical systems, fixed secondary sources are used to reproduce various desired sound fields. Therefore, the computational cost after setting the desired sound field is important in these systems, whereas other values such as $\mathbf{A}_{\mathrm{pm}}$ can be calculated beforehand. From this viewpoint, (14) can be rewritten as

$$\hat{\boldsymbol{d}}_{\mathrm{pm}} = \mathbf{C}_{\mathrm{pm}} \boldsymbol{u}_{\mathrm{des}}. \tag{17}$$

where $\boldsymbol{u}_{\mathrm{des}} \in \mathbb{C}^{M}$ is the vector of the sound pressures at the control points and $\mathbf{C}_{\mathrm{pm}} \in \mathbb{C}^{L\times M}$ is a matrix independent of the desired sound field. Since $\mathbf{C}_{\mathrm{pm}}$ can be calculated beforehand for a fixed array, the computational complexity after setting the desired sound field is $\mathcal{O}(LM)$.

### B. Mode-Matching Method

The mode-matching method aims to control the expansion coefficients of the synthesized sound field so that they correspond to the desired ones. In the reproduction of interior sound fields, the driving signals are obtained from the following mode-matching equation:

$$\mathring{u}^{\mathrm{int}}_{\mathrm{syn},\nu,\mu}(\boldsymbol{r}_{\mathrm{c}}) = \mathring{u}^{\mathrm{int}}_{\mathrm{des},\nu,\mu}(\boldsymbol{r}_{\mathrm{c}}), \quad {}^{\forall}\nu \in \{0,\ldots,N_{\mathrm{int}}\}, \tag{18}$$

where $N_{\mathrm{int}}$ is the truncation order and $\mathring{u}^{\mathrm{int}}_{syn,\nu,\mu}(\boldsymbol{r}_{\mathrm{c}})$ is the interior expansion coefficient of $u_{\mathrm{syn}}$ given as $\mathring{u}^{\mathrm{int}}_{syn,\nu,\mu}(\boldsymbol{r}_{\mathrm{c}}) = \sum_{l=1}^{L} d_l \mathring{g}^{\mathrm{int}}_{l,\nu,\mu}(\boldsymbol{r}_{\mathrm{c}})$. As shown in [3], [14], the regularized solution of (18) can be obtained by solving

$$\underset{\boldsymbol{d}\in\mathbb{C}^{L}}{\mathrm{minimize}} \quad \sum_{\nu,\mu}^{N_{\mathrm{int}}} \left| \mathring{u}^{\mathrm{int}}_{\mathrm{syn},\nu,\mu}(\boldsymbol{r}_{\mathrm{c}}) - \mathring{u}^{\mathrm{int}}_{\mathrm{des},\nu,\mu}(\boldsymbol{r}_{\mathrm{c}}) \right|^{2} + \lambda \boldsymbol{d}^{\mathsf{H}} \boldsymbol{d} \tag{19}$$

as

$$\hat{\boldsymbol{d}}_{\mathrm{mm}} = (\mathbf{A}_{\mathrm{mm}} + \lambda \boldsymbol{I}_{L})^{-1} \mathbf{b}_{\mathrm{mm}}. \tag{20}$$

Here, $\sum_{\nu,\mu}^{N_{\rm int}}$ is the abbreviated form of $\sum_{\nu=0}^{N_{\rm int}}\sum_{\mu=-\nu}^{\nu}$, and $\mathbf{A}_{\rm mm}\in\mathbb{C}^{L\times L}$ and $\mathbf{b}_{\rm mm}\in\mathbb{C}^{L}$ are given by

$$(\mathbf{A}_{\rm mm})_{l_1,l_2}=\sum_{\nu,\mu}^{N_{\rm int}}\mathring{g}_{l_1,\nu,\mu}^{\rm int}(\boldsymbol{r}_{\rm c})^*\mathring{g}_{l_2,\nu,\mu}^{\rm int}(\boldsymbol{r}_{\rm c}), \tag{21}$$

$$(\mathbf{b}_{\rm mm})_{l}=\sum_{\nu,\mu}^{N_{\rm int}}\mathring{g}_{l,\nu,\mu}^{\rm int}(\boldsymbol{r}_{\rm c})^*\mathring{u}_{{\rm des},\nu,\mu}^{\rm int}(\boldsymbol{r}_{\rm c}). \tag{22}$$

Similarly, in the reproduction of exterior sound fields, the mode-matching equation is formulated as

$$\mathring{u}_{{\rm syn},\nu,\mu}^{\rm ext}(\boldsymbol{r}_{\rm c})=\mathring{u}_{{\rm des},\nu,\mu}^{\rm ext}(\boldsymbol{r}_{\rm c}),\quad {}^{\forall}\nu\in\{0,\ldots,N_{\rm ext}\}, \tag{23}$$

where $N_{\rm ext}$ is the truncation order and $\mathring{u}_{{\rm syn},\nu,\mu}^{\rm ext}(\boldsymbol{r}_{\rm c})=\sum_{l=1}^{L}d_l\mathring{g}_{l,\nu,\mu}^{\rm ext}(\boldsymbol{r}_{\rm c})$ is the exterior expansion coefficient of $u_{\rm syn}$. Therefore, the driving signals are given by

$$\hat{\boldsymbol{d}}_{\rm mm}=\left(\mathbf{A}_{\rm mm}+\lambda\boldsymbol{I}_L\right)^{-1}\mathbf{b}_{\rm mm}, \tag{24}$$

where $\mathbf{A}_{\rm mm}\in\mathbb{C}^{L\times L}$ and $\mathbf{b}_{\rm mm}\in\mathbb{C}^{L}$ are defined as

$$(\mathbf{A}_{\rm mm})_{l_1,l_2}=\sum_{\nu,\mu}^{N_{\rm ext}}\mathring{g}_{l_1,\nu,\mu}^{\rm ext}(\boldsymbol{r}_{\rm c})^*\mathring{g}_{l_2,\nu,\mu}^{\rm ext}(\boldsymbol{r}_{\rm c}), \tag{25}$$

$$(\mathbf{b}_{\rm mm})_{l}=\sum_{\nu,\mu}^{N_{\rm ext}}\mathring{g}_{l,\nu,\mu}^{\rm ext}(\boldsymbol{r}_{\rm c})^*\mathring{u}_{{\rm des},\nu,\mu}^{\rm ext}(\boldsymbol{r}_{\rm c}). \tag{26}$$

The truncation orders $N_{\rm int}$ and $N_{\rm ext}$ are usually determined empirically according to the size of the array of the secondary sources or the reproduction region. However, it is difficult to find the optimal truncation orders, especially in interior sound field reproduction; an excessively large $N_{\rm int}$ degrades the reproduction accuracy, which can also be seen in the experiments in Section V.

Either (20) or (24) can be rewritten as

$$\hat{\boldsymbol{d}}_{\rm mm}=\mathbf{C}_{\rm mm}\mathring{\boldsymbol{u}}_{\rm des}, \tag{27}$$

where $\mathring{\boldsymbol{u}}_{\rm des}\in\mathbb{C}^{\breve{N}}$ is the vector of the interior or exterior expansion coefficients of the desired sound field and $\mathbf{C}_{\rm mm}\in\mathbb{C}^{L\times\breve{N}}$ is a matrix independent of the desired sound field. Here, $\breve{N}$ is defined as $\breve{N}=(N_{\rm int}+1)^2$ in the case of interior sound field reproduction and as $\breve{N}=(N_{\rm ext}+1)^2$ in the case of exterior sound field reproduction. Therefore, the computational complexity after setting the desired sound field is $\mathcal{O}(L\breve{N})$.

## IV. Proposed Method

In Sections IV-A and Section IV-B, the general concept of the proposed weighted mode-matching method is described. Also, we provide several examples of weights on expansion coefficients in Sections IV-C and Section IV-D. Finally, we discuss the application of the proposed method to multizone reproduction and interior sound field reproduction with exterior cancellation in Section IV-E.

### A. Formulation

The sound field reproduction problem can be formulated as minimization of the difference between the desired and synthesized sound fields. Therefore, we consider the following general formulation:

$$\underset{\boldsymbol{d}\in\mathbb{C}^L}{\text{minimize}}\quad J(\boldsymbol{d})=\|u_{\rm syn}-u_{\rm des}\|_{(*)}^2+\lambda\boldsymbol{d}^{\mathsf{H}}\boldsymbol{d}, \tag{28}$$

where $\|\cdot\|_{(*)}$ is some norm on interior or exterior sound fields induced by some inner product $\langle\cdot,\cdot\rangle_{(*)}$ as

$$\|u\|_{(*)}^2=\langle u,u\rangle_{(*)}. \tag{29}$$

A typical example of this type of norm is the $L_2$ norm with any positive spatial weight. Therefore, one can set various formulations according to the detailed objective. Several examples of norms are described in Section IV-C for interior sound fields and in Section IV-D for exterior sound fields. From (1) and (29), The objective function of (28) can be rewritten as

$$J(\boldsymbol{d})=\boldsymbol{d}^{\mathsf{H}}(\mathbf{A}_{\rm wmm}+\lambda\boldsymbol{I}_L)\boldsymbol{d}-\boldsymbol{d}^{\mathsf{H}}\mathbf{b}_{\rm wmm}-\mathbf{b}_{\rm wmm}^{\mathsf{H}}\boldsymbol{d}+{\rm c}_{\rm wmm}, \tag{30}$$

where $\mathbf{A}_{\rm wmm}\in\mathbb{C}^{L\times L}$, $\mathbf{b}_{\rm wmm}\in\mathbb{C}^{L}$, and ${\rm c}_{\rm wmm}\in[0,\infty)$ are given by

$$(\mathbf{A}_{\rm wmm})_{l_1,l_2}=\langle g_{l_1},g_{l_2}\rangle_{(*)}, \tag{31}$$

$$(\mathbf{b}_{\rm wmm})_{l}=\langle g_{l},u_{\rm des}\rangle_{(*)}, \tag{32}$$

$${\rm c}_{\rm wmm}=\langle u_{\rm des},u_{\rm des}\rangle_{(*)}. \tag{33}$$

Since $\mathbf{A}_{\rm wmm}+\lambda\boldsymbol{I}_L$ is a positive definite Hermitian matrix, i.e., $\boldsymbol{x}^{\mathsf{H}}(\mathbf{A}_{\rm wmm}+\lambda\boldsymbol{I}_L)\boldsymbol{x}>0$ for any $\boldsymbol{x}\in\mathbb{C}^L\setminus\{\mathbf{0}\}$, it has an inverse (and also positive definite Hermitian) matrix $(\mathbf{A}_{\rm wmm}+\lambda\boldsymbol{I}_L)^{-1}$. Therefore, $J$ can be represented as

$$\begin{aligned}J(\boldsymbol{d})=&\left(\boldsymbol{d}-(\mathbf{A}_{\rm wmm}+\lambda\boldsymbol{I}_L)^{-1}\mathbf{b}_{\rm wmm}\right)^{\mathsf{H}}\\&\cdot(\mathbf{A}_{\rm wmm}+\lambda\boldsymbol{I}_L)\left(\boldsymbol{d}-(\mathbf{A}_{\rm wmm}+\lambda\boldsymbol{I}_L)^{-1}\mathbf{b}_{\rm wmm}\right)\\&+{\rm c}_{\rm wmm}-\mathbf{b}_{\rm wmm}^{\mathsf{H}}(\mathbf{A}_{\rm wmm}+\lambda\boldsymbol{I}_L)^{-1}\mathbf{b}_{\rm wmm},\end{aligned} \tag{34}$$

and the optimal driving signals $\hat{\boldsymbol{d}}_{\rm wmm}\in\mathbb{C}^L$, which minimize $J$, are obtained as

$$\hat{\boldsymbol{d}}_{\rm wmm}=\left(\mathbf{A}_{\rm wmm}+\lambda\boldsymbol{I}_L\right)^{-1}\mathbf{b}_{\rm wmm}. \tag{35}$$

This can also be derived on the basis of the Wirtinger derivative, i.e., by solving $\frac{\partial}{\partial\boldsymbol{d}^{\mathsf{H}}}J(\boldsymbol{d})=\mathbf{0}$. Therefore, the remaining problem is the calculation of $\mathbf{A}_{\rm wmm}$ and $\mathbf{b}_{\rm wmm}$.

### B. Weighted Mode-Matching

Consider an inner product of two interior sound fields $u_1$ and $u_2$, i.e., $\langle u_1,u_2\rangle_{(*)}$. Let $\mathring{u}_{1,\nu,\mu}(\boldsymbol{r}_{\rm c})$ and $\mathring{u}_{2,\nu,\mu}(\boldsymbol{r}_{\rm c})$ denote respectively the interior expansion coefficients of $u_1$ and $u_2$. Then, $\langle u_1,u_2\rangle_{(*)}$ can be rewritten by assuming the interchangeability

of infinite summation and inner product[1] as

$$\begin{aligned}\langle u_1, u_2\rangle_{(*)} &= \Bigg\langle \sum_{\nu,\mu} \mathring{u}^{\mathrm{int}}_{1,\nu,\mu}(\boldsymbol{r}_{\mathrm{c}})\varphi_{\nu,\mu}(\boldsymbol{r}-\boldsymbol{r}_{\mathrm{c}}), \\ &\qquad \sum_{\nu,\mu} \mathring{u}^{\mathrm{int}}_{2,\nu,\mu}(\boldsymbol{r}_{\mathrm{c}})\varphi_{\nu,\mu}(\boldsymbol{r}-\boldsymbol{r}_{\mathrm{c}})\Bigg\rangle_{(*)} \\ &= \sum_{\nu_1,\mu_1}\sum_{\nu_2,\mu_2} \mathring{u}^{\mathrm{int}}_{1,\nu_1,\mu_1}(\boldsymbol{r}_{\mathrm{c}})^* \mathring{u}^{\mathrm{int}}_{2,\nu_2,\mu_2}(\boldsymbol{r}_{\mathrm{c}}) \\ &\qquad \cdot \langle \varphi_{\nu_1,\mu_1}, \varphi_{\nu_1,\mu_1}\rangle_{(*)}. \end{aligned} \tag{36}$$

Therefore, in interior sound field reproduction, $\mathbf{A}_{\mathrm{wmm}}$ and $\mathbf{b}_{\mathrm{wmm}}$ can be rewritten as

$$(\mathbf{A}_{\mathrm{wmm}})_{l_1,l_2} = \sum_{\nu_1,\mu_1}\sum_{\nu_2,\mu_2} w^{\nu_2,\mu_2}_{\nu_1,\mu_1} \cdot \mathring{g}^{\mathrm{int}}_{l_1,\nu_1,\mu_1}(\boldsymbol{r}_{\mathrm{c}})^* \mathring{g}^{\mathrm{int}}_{l_2,\nu_2,\mu_2}(\boldsymbol{r}_{\mathrm{c}}), \tag{37}$$

$$(\mathbf{b}_{\mathrm{wmm}})_{l} = \sum_{\nu_1,\mu_1}\sum_{\nu_2,\mu_2} w^{\nu_2,\mu_2}_{\nu_1,\mu_1} \cdot \mathring{g}^{\mathrm{int}}_{l,\nu_1,\mu_1}(\boldsymbol{r}_{\mathrm{c}})^* \mathring{u}^{\mathrm{int}}_{\mathrm{des},\nu_2,\mu_2}(\boldsymbol{r}_{\mathrm{c}}), \tag{38}$$

where $w^{\nu_2,\mu_2}_{\nu_1,\mu_1}$ are the weights on the interior expansion coefficients (referred to as the interior weights, hereafter) given as

$$w^{\nu_2,\mu_2}_{\nu_1,\mu_1} = \langle \varphi_{\nu_1,\mu_1}(\boldsymbol{r}-\boldsymbol{r}_{\mathrm{c}}), \varphi_{\nu_2,\mu_2}(\boldsymbol{r}-\boldsymbol{r}_{\mathrm{c}})\rangle_{(*)}. \tag{39}$$

In exterior sound field reproduction, on the other hand, $\mathbf{A}_{\mathrm{wmm}}$ and $\mathbf{b}_{\mathrm{wmm}}$ can be rewritten as

$$(\mathbf{A}_{\mathrm{wmm}})_{l_1,l_2} = \sum_{\nu_1,\mu_1}\sum_{\nu_2,\mu_2} v^{\nu_2,\mu_2}_{\nu_1,\mu_1} \cdot \mathring{g}^{\mathrm{ext}}_{l_1,\nu_1,\mu_1}(\boldsymbol{r}_{\mathrm{c}})^* \mathring{g}^{\mathrm{ext}}_{l_2,\nu_2,\mu_2}(\boldsymbol{r}_{\mathrm{c}}), \tag{40}$$

$$(\mathbf{b}_{\mathrm{wmm}})_{l} = \sum_{\nu_1,\mu_1}\sum_{\nu_2,\mu_2} v^{\nu_2,\mu_2}_{\nu_1,\mu_1} \cdot \mathring{g}^{\mathrm{ext}}_{l,\nu_1,\mu_1}(\boldsymbol{r}_{\mathrm{c}})^* \mathring{u}^{\mathrm{ext}}_{\mathrm{des},\nu_2,\mu_2}(\boldsymbol{r}_{\mathrm{c}}), \tag{41}$$

where $v^{\nu_2,\mu_2}_{\nu_1,\mu_1}$ are the weights on the exterior expansion coefficients (referred to as the exterior weights, hereafter) given as

$$v^{\nu_2,\mu_2}_{\nu_1,\mu_1} = \langle \psi_{\nu_1,\mu_1}(\boldsymbol{r}-\boldsymbol{r}_{\mathrm{c}}), \psi_{\nu_2,\mu_2}(\boldsymbol{r}-\boldsymbol{r}_{\mathrm{c}})\rangle_{(*)}. \tag{42}$$

Therefore, we only have to calculate the inner product on the spherical wavefunctions, i.e., $w^{\nu_2,\mu_2}_{\nu_1,\mu_1}$ and $v^{\nu_2,\mu_2}_{\nu_1,\mu_1}$, and $\mathbf{A}_{\mathrm{wmm}}$ and $\mathbf{b}_{\mathrm{wmm}}$ can be calculated for arbitrary $g_l$ and $u_{\mathrm{des}}$ using (37) and (38) or (40) and (41). Note that $w^{\nu_2,\mu_2}_{\nu_1,\mu_1}$ and $v^{\nu_2,\mu_2}_{\nu_1,\mu_1}$ are independent of $g_l$ and $u_{\mathrm{des}}$; therefore, we can calculate them beforehand analytically or numerically. Since these infinite summations are difficult to solve in many cases, the summations are truncated at a sufficiently large order $N_{\mathrm{int}}$ or $N_{\mathrm{ext}}$. Comparing (37), (38), (40), and (41) with (21), (22), (25), and (26), respectively, one can see that the difference between the proposed method and the current mode-matching method appears in the weights on the expansion coefficients, i.e., $w^{\nu_2,\mu_2}_{\nu_1,\mu_1}$ and $v^{\nu_2,\mu_2}_{\nu_1,\mu_1}$. In the proposed method, the optimal weights on the expansion coefficients are derived according to the norm to be minimized.

We also evaluate the computational cost after the desired sound field is given. Equation (35) can be rewritten in a similar form to (27) as

$$\hat{\boldsymbol{d}}_{\mathrm{wmm}} = \mathbf{C}_{\mathrm{wmm}}\mathring{\boldsymbol{u}}_{\mathrm{des}}, \tag{43}$$

where $\mathbf{C}_{\mathrm{wmm}} \in \mathbb{C}^{L\times\breve{N}}$ is independent of the desired sound field. Therefore, the computational complexity after setting the desired sound field is $\mathcal{O}(L\breve{N})$, which is the same as that of the mode-matching method.

### C. Examples of Norms on Interior Sound Fields and Their Interior Weights

We here give two examples of norms on interior sound fields and their corresponding interior weights, which are also given in Table I.

*1) Interior Uniformly Weighted $L_2$ Norm:* The first example is the interior uniformly weighted $L_2$ norm $\|\cdot\|_{\mathrm{int,uni}}$, which is defined as

$$\|u\|^2_{\mathrm{int,uni}} = \int_{\Omega_{\mathrm{int}}} |u(\boldsymbol{r})|^2\,\mathrm{d}\boldsymbol{r}. \tag{44}$$

By using this norm, one can reproduce the sound field within the spherical region $\Omega_{\mathrm{int}}$. In this case, the interior weights are obtained analytically as

$$w^{\nu_2,\mu_2}_{\nu_1,\mu_1} = \delta_{\nu_1,\nu_2}\delta_{\mu_1,\mu_2} w_{\mathrm{uni},\nu_1}, \tag{45}$$

where $\delta_{n,m}$ denotes the Kronecker's delta and

$$w_{\mathrm{uni},\nu} = 2\pi R^3_{\mathrm{int}}\left(j_\nu(kR_{\mathrm{int}})^2 - j_{\nu-1}(kR_{\mathrm{int}})j_{\nu+1}(kR_{\mathrm{int}})\right), \tag{46}$$

where $R_{\mathrm{int}}$ is the radius of the sphere $S_{\mathrm{int}}$. The proof is given in Appendix B.

*2) Interior Gaussian-Weighted $L_2$ Norm:* The second example is the interior Gaussian-weighted $L_2$ norm $\|\cdot\|_{\mathrm{int,Gs}}$, which is defined as

$$\|u\|^2_{\mathrm{int,Gs}} = \int_{\Omega_{\mathrm{int}}} \exp\left(-\frac{\|\boldsymbol{r}-\boldsymbol{r}_{\mathrm{c}}\|^2}{2\sigma^2}\right)|u(\boldsymbol{r})|^2\,\mathrm{d}\boldsymbol{r}, \tag{47}$$

where $\sigma$ is the scale parameter. Note that the Gaussian $w(\boldsymbol{r})$ is defined only on $\Omega_{\mathrm{int}}$ and truncated outside it. By using this norm, one can prioritize the reproduction around the central region while preventing significant deterioration in the peripheral region. In this case, the interior weights are obtained as

$$w^{\nu_2,\mu_2}_{\nu_1,\mu_1} = \delta_{\nu_1,\nu_2}\delta_{\mu_1,\mu_2} w_{\mathrm{Gs},\nu_1}, \tag{48}$$

where

$$\begin{aligned} w_{\mathrm{Gs},\nu} &= 4\pi\int_0^{R_{\mathrm{int}}} \exp\left(-\frac{r^2}{2\sigma^2}\right) j_\nu(kr)^2\,\mathrm{d}r, \\ &= \sum_{n=0}^{\infty}(-1)^n 2\pi R^3_{\mathrm{int}} \exp\left(-\frac{R^2_{\mathrm{int}}}{4\sigma^2}\right) i_n\left(\frac{R^2_{\mathrm{int}}}{4\sigma^2}\right) \\ &\qquad \cdot \left(j_{\nu-n}(kR_{\mathrm{int}})j_{\nu+n}(kR_{\mathrm{int}}) \right. \\ &\qquad \left. - j_{\nu-n-1}(kR_{\mathrm{int}})j_{\nu+n+1}(kR_{\mathrm{int}})\right), \end{aligned} \tag{49}$$

[1]The interchangeability of infinite summation and inner product holds if the spherical wavefunction expansion of sound fields converges with respect to the norm $\|\cdot\|_{(*)}$ (see Appendix A for the proof). However, this condition is satisfied in almost any practical case (at least when the norm $\|u\|_{(*)}$ consists of the integral of $u$ and its partial derivatives on a compact set) including all examples shown in Sections IV-C and Section IV-D. This is because the spherical wavefunction expansion of the interior sound field and its partial derivatives converge uniformly in $\Omega_{\mathrm{int}}$ and the spherical wavefunction expansion of the exterior sound field and its partial derivatives converge uniformly in any compact subset of $\Omega_{\mathrm{ext}}$ [23].

TABLE I
EXAMPLES OF NORMS ON INTERIOR SOUND FIELDS AND THEIR INTERIOR WEIGHTS

| Norm on interior sound fields | Interior weights |
|---|---|
| Interior uniformly weighted $L_2$ norm: $\|u\|^2_{\mathrm{int,uni}} = \int_{\Omega_{\mathrm{int}}} \lvert u(\boldsymbol{r})\rvert^2 \,\mathrm{d}\boldsymbol{r}$ | $w_{\mathrm{uni},\nu} = 2\pi R^3_{\mathrm{int}} \left(j_\nu(kR_{\mathrm{int}})^2 - j_{\nu-1}(kR_{\mathrm{int}})j_{\nu+1}(kR_{\mathrm{int}})\right)$ |
| Interior Gaussian-weighted $L_2$ norm: $\|u\|^2_{\mathrm{int,Gs}} = \int_{\Omega_{\mathrm{int}}} \exp\left(-\frac{\lVert\boldsymbol{r}-\boldsymbol{r}_{\mathrm{c}}\rVert^2}{2\sigma^2}\right) \lvert u(\boldsymbol{r})\rvert^2 \,\mathrm{d}\boldsymbol{r}$ | $w_{\mathrm{Gs},\nu} = \sum_{n=0}^{\infty}(-1)^n 2\pi R^3_{\mathrm{int}} \exp\left(-\frac{R^2_{\mathrm{int}}}{4\sigma^2}\right) i_n\left(\frac{R^2_{\mathrm{int}}}{4\sigma^2}\right) \cdot \left(j_{\nu-n}(kR_{\mathrm{int}})j_{\nu+n}(kR_{\mathrm{int}}) - j_{\nu-n-1}(kR_{\mathrm{int}})j_{\nu+n+1}(kR_{\mathrm{int}})\right)$ |

TABLE II
EXAMPLES OF NORMS ON EXTERIOR SOUND FIELDS AND THEIR EXTERIOR WEIGHTS

| Norm on exterior sound fields | Exterior weights |
|---|---|
| Exterior uniformly weighted $L_2$ norm: $\|u\|^2_{\mathrm{ext,uni}} = \int_{\Omega'_{\mathrm{ext}}} \lvert u(\boldsymbol{r})\rvert^2 \,\mathrm{d}\boldsymbol{r}$ | $v_{\mathrm{uni},\nu} = 2\pi R'^3_{\mathrm{ext}} \left(\lvert h_\nu(kR'_{\mathrm{ext}})\rvert^2 - h_{\nu-1}(kR'_{\mathrm{ext}})^* h_{\nu+1}(kR'_{\mathrm{ext}})\right) - 2\pi R^3_{\mathrm{ext}} \left(\lvert h_\nu(kR_{\mathrm{ext}})\rvert^2 - h_{\nu-1}(kR_{\mathrm{ext}})^* h_{\nu+1}(kR_{\mathrm{ext}})\right)$ |
| Exterior radiation-power norm: $\|u\|^2_{\mathrm{ext,rad}} = \int_{S_{\mathrm{ext}}} \frac{1}{2}\mathrm{Re}\left[u(\boldsymbol{r})\frac{\mathrm{j}}{\rho ck}\frac{\partial}{\partial\hat{\boldsymbol{n}}(\boldsymbol{r})}u(\boldsymbol{r})^*\right] \mathrm{d}\boldsymbol{r}$ | $v_{\mathrm{rad},\nu} = \frac{2\pi}{\rho ck^2}$ |

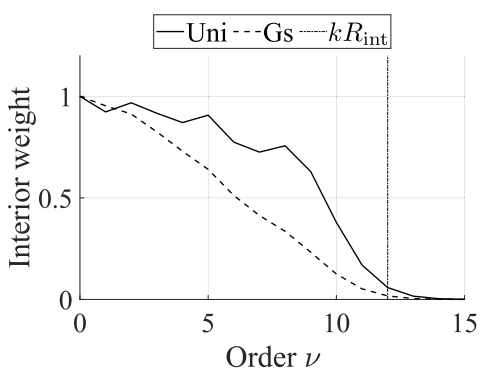


Fig. 2. Example of interior weights for interior uniformly weighted $L_2$ norm (Uni) and interior Gaussian-weighted $L_2$ norm (Gs).

where $i_n(\cdot)$ is the $n$th-order modified spherical Bessel function of the first kind [24]. The derivation is given in Appendix C. Although there is no useful formula to evaluate the integral in the first line of (49), it can be calculated efficiently by truncating the second line at sufficiently large $n$.

In both examples, the orthogonality of the interior spherical wavefunctions holds as in (45) and (48). Therefore, (37) and (38) can be rewritten as

$$(\mathbf{A}_{\mathrm{wmm}})_{l_1,l_2} = \sum_{\nu,\mu} w_{(*),\nu} \mathring{g}^{\mathrm{int}}_{l_1,\nu,\mu}(\boldsymbol{r}_{\mathrm{c}})^* \mathring{g}^{\mathrm{int}}_{l_2,\nu,\mu}(\boldsymbol{r}_{\mathrm{c}}), \tag{50}$$

$$(\mathbf{b}_{\mathrm{wmm}})_{l} = \sum_{\nu,\mu} w_{(*),\nu} \mathring{g}^{\mathrm{int}}_{l,\nu,\mu}(\boldsymbol{r}_{\mathrm{c}})^* \mathring{u}^{\mathrm{int}}_{\mathrm{des},\nu,\mu}(\boldsymbol{r}_{\mathrm{c}}), \tag{51}$$

where $w_{(*),\nu}$ represents either $w_{\mathrm{uni},\nu}$ or $w_{\mathrm{Gs},\nu}$. As an example, the values of $w_{\mathrm{uni},\nu}$ or $w_{\mathrm{Gs},\nu}$ are plotted in Fig. 2 in the case of $k = 10$ rad/m, $R_{\mathrm{int}} = 1.2$ m, and $\sigma = 0.6$ m. Here, the weights are normalized so that their zeroth-order values correspond to one.

### *D. Examples of Norms on Exterior Sound Fields and Their Exterior Weights*

We also give two examples of norms on exterior sound fields and their exterior weights, which are also given in Table II.

*1) Exterior Uniformly Weighted $L_2$ Norm:* The first example is the exterior uniformly weighted $L_2$ norm $\|\cdot\|_{\mathrm{ext,uni}}$, which is defined as

$$\|u\|^2_{\mathrm{ext,uni}} = \int_{\Omega'_{\mathrm{ext}}} \lvert u(\boldsymbol{r})\rvert^2 \,\mathrm{d}\boldsymbol{r}. \tag{52}$$

Here, $\Omega'_{\mathrm{ext}} \subset \Omega_{\mathrm{ext}}$ is defined as the region between the inner sphere $S_{\mathrm{ext}}$ and the outer sphere $S'_{\mathrm{ext}}$, which is also centered at $\boldsymbol{r}_{\mathrm{c}}$. By using this norm, one can reproduce the sound field within the region $\Omega'_{\mathrm{ext}}$. In this case, the exterior weights are obtained analytically as

$$v^{\nu_2,\mu_2}_{\nu_1,\mu_1} = \delta_{\nu_1,\nu_2}\delta_{\mu_1,\mu_2} v_{\mathrm{uni},\nu_1}, \tag{53}$$

where

$$\begin{aligned} v_{\mathrm{uni},\nu} = {} & 2\pi R'^3_{\mathrm{ext}} \left(\lvert h_\nu(kR'_{\mathrm{ext}})\rvert^2 - h_{\nu-1}(kR'_{\mathrm{ext}})^* h_{\nu+1}(kR'_{\mathrm{ext}})\right) \\ & - 2\pi R^3_{\mathrm{ext}} \left(\lvert h_\nu(kR_{\mathrm{ext}})\rvert^2 - h_{\nu-1}(kR_{\mathrm{ext}})^* h_{\nu+1}(kR_{\mathrm{ext}})\right). \end{aligned} \tag{54}$$

Here, $R_{\mathrm{ext}}$ and $R'_{\mathrm{ext}}$ are the radii of $S_{\mathrm{ext}}$ and $S'_{\mathrm{ext}}$, respectively. The derivation is given in Appendix D.

*2) Exterior Radiation-Power Norm:* The second example is the exterior radiation-power norm $\|\cdot\|_{\mathrm{ext,rad}}$, which is defined as

$$\|u\|^2_{\mathrm{ext,rad}} = \int_{S_{\mathrm{ext}}} \frac{1}{2}\mathrm{Re}\left[u(\boldsymbol{r})\frac{\mathrm{j}}{\rho ck}\frac{\partial}{\partial\hat{\boldsymbol{n}}(\boldsymbol{r})}u(\boldsymbol{r})^*\right] \mathrm{d}\boldsymbol{r}, \tag{55}$$

where $\mathrm{Re}[\cdot]$ denotes the real part of a complex value, $\rho$ is the density of air, and $\partial/\partial\hat{\boldsymbol{n}}(\boldsymbol{r})$ denotes the outward normal derivative. Since the integrand of (55) represents the outward acoustic intensity [33], this norm corresponds to the total power

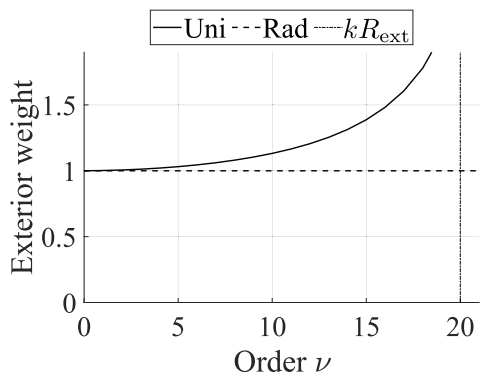


Fig. 3. Example of exterior weights for exterior uniformly weighted $L_2$ norm (Uni) and exterior radiation-power norm (Rad).

radiated outside $S_{\rm ext}$. In this case, the exterior weights are obtained analytically as

$$v_{\nu_1,\mu_1}^{\nu_2,\mu_2} = \delta_{\nu_1,\nu_2}\delta_{\mu_1,\mu_2} v_{{\rm rad},\nu_1}, \tag{56}$$

where

$$v_{{\rm rad},\nu} = \frac{2\pi}{\rho c k^2}. \tag{57}$$

The derivation is given in Appendix E.

In both examples, the orthogonality of the exterior spherical wavefunctions holds as in (53) and (56). Therefore, (40) and (41) can be rewritten as

$$(\mathbf{A}_{\rm wmm})_{l_1,l_2} = \sum_{\nu,\mu} v_{(*),\nu} \mathring{g}_{l_1,\nu,\mu}^{\rm ext}(\boldsymbol{r}_{\rm c})^* \mathring{g}_{l_2,\nu,\mu}^{\rm ext}(\boldsymbol{r}_{\rm c}), \tag{58}$$

$$(\mathbf{b}_{\rm wmm})_l = \sum_{\nu,\mu} v_{(*),\nu} \mathring{g}_{l,\nu,\mu}^{\rm ext}(\boldsymbol{r}_{\rm c})^* \mathring{u}_{{\rm des},\nu,\mu}^{\rm ext}(\boldsymbol{r}_{\rm c}), \tag{59}$$

where $v_{(*),\nu}$ represents either $v_{{\rm uni},\nu}$ or $v_{{\rm rad},\nu}$. As an example, the values of $v_{{\rm uni},\nu}$ or $v_{{\rm rad},\nu}$ are plotted in Fig. 3 in the case of $k = 10$ rad/m, $R_{\rm ext} = 2.0$ m, and $R'_{\rm ext} = 2.5$ m. Here, the weights are normalized so that their zeroth-order values correspond to one.

Furthermore, in the case of the exterior radiation-power norm, (58) and (59) can be calculated analytically without infinite summations as follows. Suppose each $g_l$ and $u_{\rm des}$ are modeled by the finite-order exterior spherical wavefunctions around their source positions $\boldsymbol{r}_l$ and $\boldsymbol{r}_{\rm des}$ (e.g., monopole, dipole, and cardioid sources) as

$$g_l(\boldsymbol{r}) = \sum_{\nu,\mu}^{N_l} \beta_{l,\nu,\mu}\psi_{\nu,\mu}(\boldsymbol{r}-\boldsymbol{r}_l), \tag{60}$$

$$u_{\rm des}(\boldsymbol{r}) = \sum_{\nu,\mu}^{N_{\rm des}} \beta_{{\rm des},\nu,\mu}\psi_{\nu,\mu}(\boldsymbol{r}-\boldsymbol{r}_{\rm des}). \tag{61}$$

In this case, $\mathbf{A}_{\rm wmm}$ and $\mathbf{b}_{\rm wmm}$ are derived analytically as

$$(\mathbf{A}_{\rm wmm})_{l_1,l_2} = \frac{2\pi}{\rho c k^2} \sum_{\nu_1,\mu_1}^{N_{l_1}} \sum_{\nu_2,\mu_2}^{N_{l_2}} T_{\nu_1,\mu_1}^{\nu_2,\mu_2}(\boldsymbol{r}_{l_1}-\boldsymbol{r}_{l_2}) \beta_{l_1,\nu_1,\mu_1}^* \beta_{l_2,\nu_2,\mu_2}, \tag{62}$$

$$(\mathbf{b}_{\rm wmm})_l = \frac{2\pi}{\rho c k^2} \sum_{\nu_1,\mu_1}^{N_l} \sum_{\nu_2,\mu_2}^{N_{\rm des}} T_{\nu_1,\mu_1}^{\nu_2,\mu_2}(\boldsymbol{r}_l-\boldsymbol{r}_{\rm des}) \cdot \beta_{l,\nu_1,\mu_1}^* \beta_{{\rm des},\nu_2,\mu_2}. \tag{63}$$

The derivation is given in Appendix E. Note that $\mathbf{A}_{\rm wmm}$ and $\mathbf{b}_{\rm wmm}$ do not depend on $\boldsymbol{r}_{\rm c}$ or $R_{\rm ext}$ in this case; they are determined only by the relative positions and directivities of the secondary and desired sources.

### E. Several Applications

In the above sections, only a single norm is used to formulate the minimization problem; however, we can formulate various minimization problems by combining multiple norms. Although there are various possible applications, we here discuss two examples: multizone reproduction and interior reproduction with exterior cancellation.

*1) Multizone Reproduction:* Multizone reproduction aims to reproduce different sound fields in different listening areas. Let $q = 1, \ldots, Q$ be the index of the listening area, $\Omega_{\rm int}^{(q)}$ be the $q$th listening area, which is a spherical region centered at $\boldsymbol{r}_{\rm c}^{(q)}$, and $u_{\rm des}^{(q)}$ denote the desired interior sound field in the $q$th listening area. Then, the multizone reproduction is formulated as

$$\underset{\boldsymbol{d}\in\mathbb{C}^L}{\text{minimize}} \quad J(\boldsymbol{d}) = \sum_{q=1}^{Q} \gamma_q \|u_{\rm syn} - u_{\rm des}^{(q)}\|_{(q)}^2 + \lambda \boldsymbol{d}^{\mathsf{H}}\boldsymbol{d}, \tag{64}$$

where $\|\cdot\|_{(q)}$ is the norm on the interior sound fields defined on $\Omega_{\rm int}^{(q)}$ and $\gamma_q$ is a constant parameter used to balance the $Q$ norms. In this case, the optimal driving signals are obtained as

$$\hat{\boldsymbol{d}} = \left(\sum_{q=1}^{Q} \gamma_q \mathbf{A}^{(q)} + \lambda \boldsymbol{I}_L\right)^{-1} \sum_{q=1}^{Q} \gamma_q \mathbf{b}^{(q)}, \tag{65}$$

where $\mathbf{A}^{(q)}$ and $\mathbf{b}^{(q)}$ are derived for each $q$ with a different expansion center $\boldsymbol{r}_{\rm c}^{(q)}$.

*2) Interior Reproduction With Exterior Cancellation:* In the reproduction of interior sound fields in reverberant environments, it is useful to suppress the exterior radiation outside the secondary sources to prevent the performance degradation caused by reverberation. This can be formulated as follows:

$$\underset{\boldsymbol{d}\in\mathbb{C}^L}{\text{minimize}} \quad J(\boldsymbol{d}) = \|u_{\rm syn} - u_{\rm des}\|_{{\rm int},(*)}^2 + \eta\|u_{\rm syn}\|_{{\rm ext},(*)}^2 + \lambda \boldsymbol{d}^{\mathsf{H}}\boldsymbol{d}, \tag{66}$$

where $\|\cdot\|_{{\rm int},(*)}$ is some norm on interior sound fields, $\|\cdot\|_{{\rm ext},(*)}$ is some norm on exterior sound fields, and $\eta$ is a constant parameter used to balance the two norms. In this case, the optimal driving signals are obtained as

$$\hat{\boldsymbol{d}} = (\mathbf{A}_{\rm int} + \eta\mathbf{A}_{\rm ext} + \lambda\boldsymbol{I}_L)^{-1}\mathbf{b}_{\rm int}, \tag{67}$$

where $\mathbf{A}_{\rm int}$ and $\mathbf{b}_{\rm int}$ are respectively given by (37) and (38) on the basis of the norm $\|\cdot\|_{{\rm int},(*)}$ and $\mathbf{A}_{\rm ext}$ is given by (40) on the basis of the norm $\|\cdot\|_{{\rm ext},(*)}$.

## V. Numerical Experiments

Numerical simulations were conducted to evaluate the proposed method in comparison with the pressure-matching method [11] and the mode-matching method [13]. Hereafter, the proposed method, the pressure-matching method, and the mode-matching method are denoted by **Proposed**, **PM**, and **MM**, respectively.

### *A. Interior Sound Field Reproduction Using Cardioid Loudspeaker Array*

In Cartesian coordinates $\boldsymbol{r} = (x, y, z)$, 144 secondary sources were located on a sphere with a radius of 1.5 m centered at $(0, 0, 0)$ m.

The positions of the secondary sources were determined on the basis of the spherical $t$-design [34]. Each secondary source was modeled as a fixed-directivity first-order source, whose transfer function is given by [14]

$$g_l(\boldsymbol{r}) = \frac{\exp(\mathrm{j}k\|\boldsymbol{r}-\boldsymbol{r}_l\|)}{4\pi\|\boldsymbol{r}-\boldsymbol{r}_l\|} \cdot \left[\alpha - (1-\alpha)\left(1 + \frac{\mathrm{j}}{k\|\boldsymbol{r}-\boldsymbol{r}_l\|}\right)\cos\gamma_l\right], \quad (68)$$

where $\alpha$ is a directivity parameter and $\gamma_l$ represents the angle between $\boldsymbol{r} - \boldsymbol{r}_l$ and the highest-gain direction of the secondary source, denoted by $\hat{\boldsymbol{p}}_l$. The directivity parameters were set as $\alpha = 0.5$ (i.e., cardioid source) and the highest-gain directions are oriented to the center of the sphere, i.e., $\hat{\boldsymbol{p}}_l = -\hat{\boldsymbol{r}}_l$, where $\hat{\boldsymbol{r}}_l = \boldsymbol{r}_l/\|\boldsymbol{r}_l\|$. Then, $g_l$ can be represented as [14]

$$g_l(\boldsymbol{r}) = \sum_{\nu,\mu} \beta_{l,\nu,\mu}\psi_{\nu,\mu}(\boldsymbol{r}-\boldsymbol{r}_l) \quad (69)$$

with

$$\beta_{l,\nu,\mu} = \begin{cases} \alpha\frac{\mathrm{j}k}{\sqrt{4\pi}}, & \nu = 0 \\ (1-\alpha)kY_{1,\mu}(-\hat{\boldsymbol{p}}_l)^*, & \nu = 1 \\ 0, & \nu \geq 2 \end{cases}. \quad (70)$$

The desired sound field was a plane wave propagating in the positive $x$-direction, i.e., $u_{\mathrm{des}}(\boldsymbol{r}) = a\exp(\mathrm{j}kx)$, where the amplitude was set as $a = 1$. The sound speed was set as 340.29 m/s.

In **Proposed** and **MM**, the center of the spherical wavefunction expansion was set at $\boldsymbol{r}_{\mathrm{c}} = (0, 0, 0)$ m. The interior expansion coefficients of the secondary sources were calculated using (70) and (12), and the interior expansion coefficients of the desired sound field were calculated as [3]

$$\mathring{u}^{\mathrm{int}}_{\mathrm{des},\nu,\mu}(\boldsymbol{r}_{\mathrm{c}}) = a\sqrt{4\pi}\mathrm{j}^{\nu}Y_{\nu,\mu}(\hat{\boldsymbol{r}}_x)^*, \quad (71)$$

where $\hat{\boldsymbol{r}}_x$ is the unit direction vector along the positive $x$-direction. Several truncation orders $N_{\mathrm{int}}$ were used in **Proposed** and **MM**. In **Proposed**, the two norms described in Section IV-C, i.e., $\|\cdot\|_{\mathrm{int,uni}}$ and $\|\cdot\|_{\mathrm{int,Gs}}$, were evaluated, which are hereafter denoted by **Proposed (Uni)** and **Proposed (Gs)**, respectively. The radius of $S_{\mathrm{int}}$ was set as $R_{\mathrm{int}} = 1.2$ m, and the scale parameter $\sigma$ in **Proposed (Gs)** was set as 0.3 m. In **PM**, the control points were aligned in a grid at regular intervals in all three directions within $\Omega_{\mathrm{int}}$, where various intervals were evaluated. The regularization parameter $\lambda$ was set as $\lambda = 10^{-3} \times \|\mathbf{A}\|_2$ in all the methods, where $\|\mathbf{A}\|_2$ denotes the maximum singular value of $\mathbf{A}$ and $\mathbf{A}$ represents $\mathbf{A}_{\mathrm{wmm}}$, $\mathbf{A}_{\mathrm{mm}}$, and $\mathbf{A}_{\mathrm{pm}}$ for **Proposed**, **MM**, and **PM**, respectively.

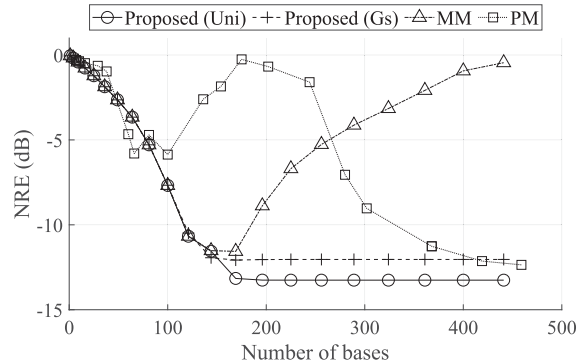


Fig. 4. Normalized reproduction error (NRE) plotted against number of basis functions at 550 Hz when plane wave propagating in positive $x$-direction is reproduced by using spherical array of 144 cardioid sources oriented inward.

To evaluate the reproduction accuracy, we define the normalized reproduction error (NRE) as

$$\mathrm{NRE}(\omega) = 10\log_{10}\frac{\int_{\Omega_{\mathrm{int}}}|u_{\mathrm{syn}}(\boldsymbol{r},\omega) - u_{\mathrm{des}}(\boldsymbol{r},\omega)|^2\,\mathrm{d}\boldsymbol{r}}{\int_{\Omega_{\mathrm{int}}}|u_{\mathrm{des}}(\boldsymbol{r},\omega)|^2\,\mathrm{d}\boldsymbol{r}}\ (\mathrm{dB}), \quad (72)$$

where the spatial integrals were discretized with an interval of 0.05 m. Note that small NRE indicates high reproduction performance.

First, we plotted the relationship of the reproduction accuracy to the number of basis functions, i.e., $\breve{N}$ for **Proposed** and **MM** and $M$ for **PM**, at 550 Hz in Fig. 4. **Proposed** and **MM** achieved almost the same NREs for a small number of basis functions. However, the NRE for **MM** rapidly increased when the number of basis functions exceeded 169, i.e., $N_{\mathrm{int}} > 12$. This is considered to be because the same weightings are imposed on all the modes. From the properties of the spherical Bessel functions of the first kind [3], spherical wavefunctions of high orders tend to have small values within $\Omega_{\mathrm{int}}$. When large $N_{\mathrm{int}}$ is used, a relatively large effort is devoted to matching these insignificant modes, and the significant low-order modes are undervalued in the **MM**, which causes the increase of the NREs. Note that the optimal $N_{\mathrm{int}} = 12$ for **MM** does not correspond to either $\lceil kR_{\mathrm{int}}\rceil = 10$ or $\lceil (e/2)kR_{\mathrm{int}}\rceil = 14$, which are two commonly used rules of thumb on the truncation [3], [21]. Therefore, it can be seen that one has to evaluate many different $N_{\mathrm{int}}$ in **MM** to achieve the best performance. On the other hand, **Proposed** is not affected by $N_{\mathrm{int}}$ as long as it is sufficiently large. This is an important point because it implies that the tuning of $N$ required in **MM** is unnecessary in **Proposed**, which can result in less total complexity of computation. Although the NREs for **Proposed (Uni)** and **PM** were close for a large number of basis functions, that for **Proposed(Uni)** reached its peak at a relatively smaller number of basis functions than that for **PM**. This means

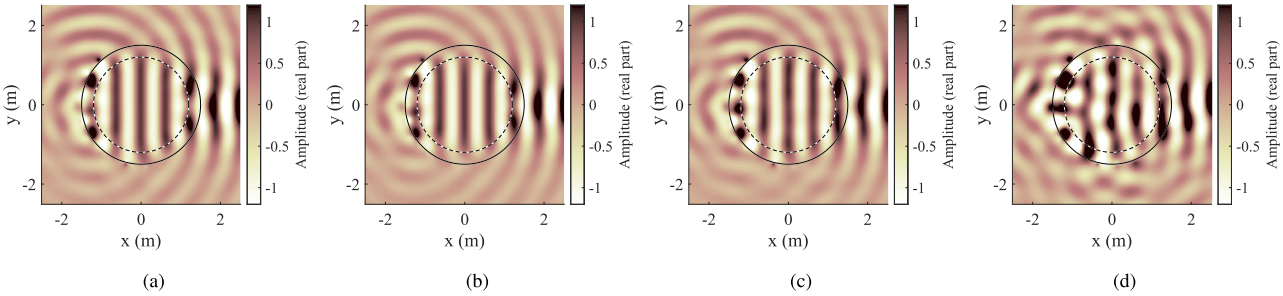


Fig. 5. Reproduced sound pressure distributions at 550 Hz when plane wave propagating in positive $x$-direction is reproduced using spherical array of 144 cardioid sources oriented inward. (a) **Proposed (Uni)**; (b) **Proposed (Gs)**; (c) **MM**; (d) **PM**.

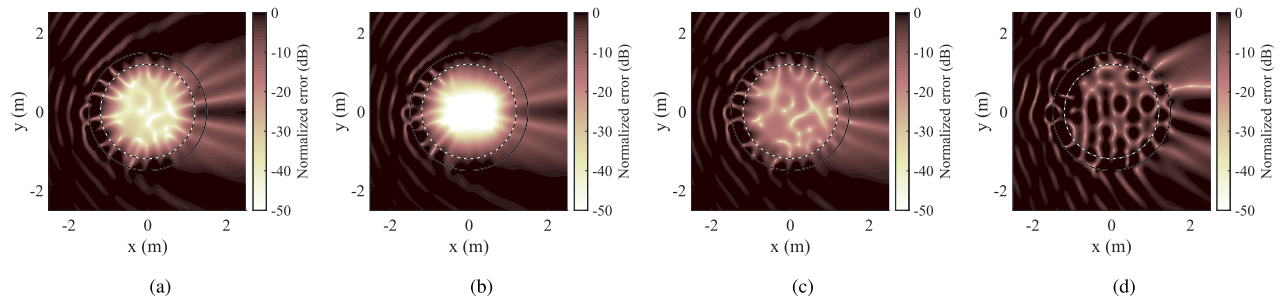


Fig. 6. Normalized error distributions at 550 Hz when plane wave propagating in positive $x$-direction is reproduced using spherical array of 144 cardioid sources oriented inward. (a) **Proposed (Uni)**; (b) **Proposed (Gs)**; (c) **MM**; (d) **PM**.

that a lower computational cost can be achieved for **Proposed** than that for **PM**.

Figs. 5 and 6 respectively show the reproduced sound pressure distributions and the normalized error distributions at 550 Hz. The solid lines and dashed lines represent the sphere where secondary sources exist and the reproduction region $\Omega_{\mathrm{int}}$, respectively. In addition, we plotted NREs against distance from the center of the array defined as

$$\mathrm{NRE}(r,\omega) = 10\log_{10}\frac{\int_{\mathbb{S}^2}|u_{\mathrm{des}}(r\hat{\boldsymbol{r}},\omega)-u_{\mathrm{syn}}(r\hat{\boldsymbol{r}},\omega)|^2\,\mathrm{d}\hat{\boldsymbol{r}}}{\int_{\mathbb{S}^2}|u_{\mathrm{des}}(r\hat{\boldsymbol{r}},\omega)|^2\,\mathrm{d}\hat{\boldsymbol{r}}}\ (\mathrm{dB}) \quad (73)$$

in Fig. 7. Here, $\mathbb{S}^2$ denotes the unit sphere and the integral was calculated by Monte Carlo integration using 500 points sampled from the spherical uniform distribution. On the basis of the result in Fig. 4, truncation orders were determined here as $N_{\mathrm{int}} = 12$ in **Proposed** and **MM**. In **PM**, the interval of the control points was set as 0.35 m so that the number of control points slightly exceeded the number of basis functions of the other methods, i.e., $M = 175$ and $\breve{N} = 169$. The NREs of **Proposed (Uni)**, **Proposed (Gs)**, **MM**, and **PM** were $-13.16$, $-12.08$, $-11.56$, and $-0.26$ dB, respectively. **Proposed (Uni)** achieved the lowest NRE, and its reproduction accuracy was relatively uniformly high within $\Omega_{\mathrm{int}}$. On the other hand, $\mathbf{Proposed(Gs)}$ achieved much higher reproduction accuracy around the central region of $\Omega_{\mathrm{int}}$ than the other methods. This is due to the interior weights based on the norm $\|\cdot\|_{\mathrm{G}s}$.

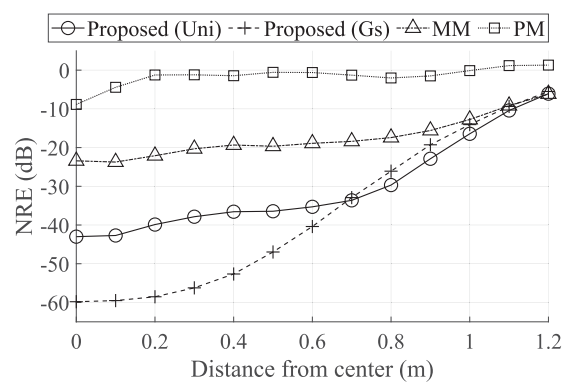


Fig. 7. Normalized reproduction error (NRE) plotted against distance from center at 550 Hz when plane wave propagating in positive $x$-direction is reproduced by using spherical array of 144 cardioid sources oriented inward.

The NRE is also plotted against frequency from 50 Hz to 800 Hz at intervals of 50 Hz in Fig. 8. Since it will take a high computational cost to seek the optimal $N_{\mathrm{int}}$ at each frequency, especially in **MM**, two rules of thumb, $N_{\mathrm{int}} = \lceil kR_{\mathrm{int}} \rceil$ and $N_{\mathrm{int}} = \lceil (e/2)kR_{\mathrm{int}} \rceil$, were investigated in **MM**. In **Proposed**, $N_{\mathrm{int}}$ was set as $\lceil (e/2)kR_{\mathrm{int}} \rceil$, and the number of control points in **PM** was determined so that it was equal to or slightly larger than $\breve{N}$ for **Proposed**. **Proposed (Gs)** was omitted here since it does not aim the uniformly high reproduction accuracy within $\Omega_{\mathrm{int}}$. Again, it can be seen the performance of **MM** depends heavily on the truncation order. Note that superiority and inferiority between two rules differ by frequencies, which implies

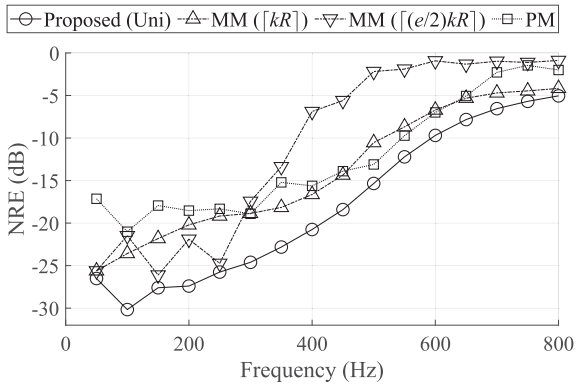


Fig. 8. Normalized reproduction error (NRE) plotted against frequency when plane wave propagating in positive $x$-direction is reproduced by using spherical array of 144 cardioid sources oriented inward.

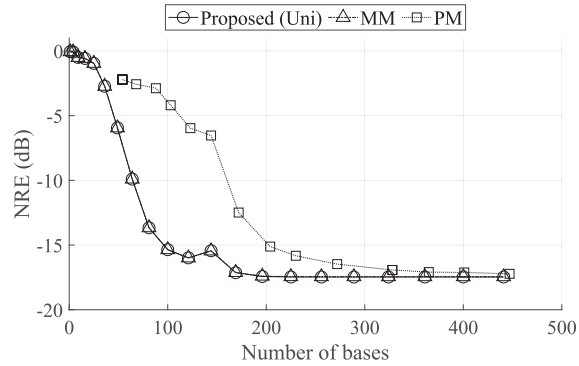


Fig. 9. Nomalized reproduction error (NRE) plotted against number of basis functions at 400 Hz when spherical wave from point source at $(1.0, 0, 0)$ m is reproduced by using spherical array of 144 cardioid sources oriented outward.

the complexity of tuning of $N_{\mathrm{int}}$ in **MM**. Without such tuning of $N_{\mathrm{int}}$, **Proposed (Uni)** achieved the lowest NRE at all the frequencies. This is due to the optimal weighting on the interior expansion coefficients determined analytically on the basis of the norm on the sound fields.

### *B. Exterior Sound Field Reproduction Using Cardioid Loudspeaker Array*

We also conducted a simulation of exterior sound field reproduction. In this experiment, 144 cardioid sources were located at the same position as in Section V-A, and each cardioid source was oriented outward from the center of the array, i.e, $\hat{\boldsymbol{p}}_l = \hat{\boldsymbol{r}}_l$. The desired sound field was a spherical wave from a point source at $\boldsymbol{r}_{\mathrm{des}} = (1.0, 0, 0)$ m, i.e., $u_{\mathrm{des}}(\boldsymbol{r}) = a\ \exp(\mathrm{j}k\|\boldsymbol{r} - \boldsymbol{r}_{\mathrm{des}}\|)/4\pi\|\boldsymbol{r} - \boldsymbol{r}_{\mathrm{des}}\|$, where the amplitude was set as $a = 10$.

In **Proposed** and **MM**, the center of the spherical wave-function expansion was set at $\boldsymbol{r}_c = (0, 0, 0)$ m. The exterior expansion coefficients of the secondary sources were calculated using (70) and (11), and the exterior expansion coefficients of the desired sound field were calculated as [3]

$$\mathring{u}^{\mathrm{ext}}_{\mathrm{des},\nu,\mu}(\boldsymbol{r}_{\mathrm{c}}) = a\frac{\mathrm{j}k}{\sqrt{4\pi}} j_\nu(kr_{\mathrm{des}}) Y_{\nu,\mu}(\hat{\boldsymbol{r}}_{\mathrm{des}})^*, \tag{74}$$

where $r_{\mathrm{des}} = \|\boldsymbol{r}_{\mathrm{des}}\|$ and $\hat{\boldsymbol{r}}_{\mathrm{des}} = \boldsymbol{r}_{\mathrm{des}}/r_{\mathrm{des}}$. Several truncation orders $N_{\mathrm{ext}}$ were used in **Proposed** and **MM**. In **Proposed**, the two norms described in Section IV-D, i.e., $\|\cdot\|_{\mathrm{ext,uni}}$ and $\|\cdot\|_{\mathrm{ext,rad}}$, were evaluated, which are hereafter denoted by **Proposed (Uni)** and **Proposed (Rad)**, respectively. In **Proposed (Uni)**, the radii of $S_{\mathrm{ext}}$ and $S'_{\mathrm{ext}}$ were respectively set as $R_{\mathrm{ext}} = 2.0$ m and $R_{\mathrm{ext}} = 2.5$ m. In **Proposed (Rad)**, $\mathbf{A}_{\mathrm{wmm}}$ and $\mathbf{b}_{\mathrm{wmm}}$ were calculated analytically using (62) and (63). In **PM**, the control points were aligned in a grid at regular intervals in all three directions within $\Omega'_{\mathrm{ext}}$, where various intervals were evaluated. The regularization parameter $\lambda$ was set as $\lambda = 10^{-3} \times \|\mathbf{A}\|_2$ in all the methods. To evaluate the reproduction accuracy, we define the NRE as

$$\mathrm{NRE}(\omega) = 10\log_{10}\frac{\int_{\Omega'_{\mathrm{ext}}} |u_{\mathrm{syn}}(\boldsymbol{r},\omega) - u_{\mathrm{des}}(\boldsymbol{r},\omega)|^2\,\mathrm{d}\boldsymbol{r}}{\int_{\Omega'_{\mathrm{ext}}} |u_{\mathrm{des}}(\boldsymbol{r},\omega)|^2\,\mathrm{d}\boldsymbol{r}}\ (\mathrm{dB}), \tag{75}$$

where the spatial integrals were discretized with an interval of 0.05 m.

First, we plotted the relationship of the reproduction accuracy to the number of basis functions at 400 Hz in Fig. 9. **Proposed (Rad)** was omitted because no truncation was used in it. In this case, the NREs for **Proposed (Uni)** and **MM** were almost the same, and the NRE for **MM** did not increase as $N_{\mathrm{ext}}$ increased. Note that **MM** corresponds to **Proposed (Rad)** as $N_{\mathrm{ext}} \to \infty$. As in the interior sound field reproduction, **Proposed** and **MM** achieved their maximum performance at a smaller number of basis functions than **PM**.

Figs. 10 and 11 respectively show the reproduced sound pressure distributions and the normalized error distributions at 400 Hz. The dashed lines represent the reproduction region $\Omega'_{\mathrm{ext}}$. On the basis of the result in Fig. 9, the truncation order was determined as $N_{\mathrm{ext}} = 13$ in **Proposed (Uni)** and **MM**. In **PM**, the interval of control points was set as 0.55 m so that the number of control points slightly exceeded the number of basis functions of the other methods, i.e., $M = 204$ and $\breve{N} = 196$. The NREs for **Proposed (Uni)**, **Proposed (Rad)**, **MM**, and **PM** were $-17.43$, $-17.45$, $-17.40$, and $-15.12$ dB. The NREs for all the methods were close; however, **Proposed (Rad)** achieved the lowest value.

The NRE is also plotted against frequency from 50 Hz to 800 Hz at intervals of 50 Hz in Fig. 12. Here, the truncation order was set as $N_{\mathrm{ext}} = \lceil (e/2)kR_{\mathrm{ext}} \rceil$ in **Proposed (Uni)** and **MM**. The number of control points in **PM** was determined so that it was equal to or slightly larger than $\breve{N}$ for the other methods. It can be seen that **Proposed (Uni)** achieved higher performance than the other methods, especially at low frequencies.

### *C. Multizone Reproduction With Exterior Cancellation Using Omnidirectional Loudspeaker Array*

Finally, we evaluate **Proposed** for multizone reproduction with exterior cancellation using a monopole array. The

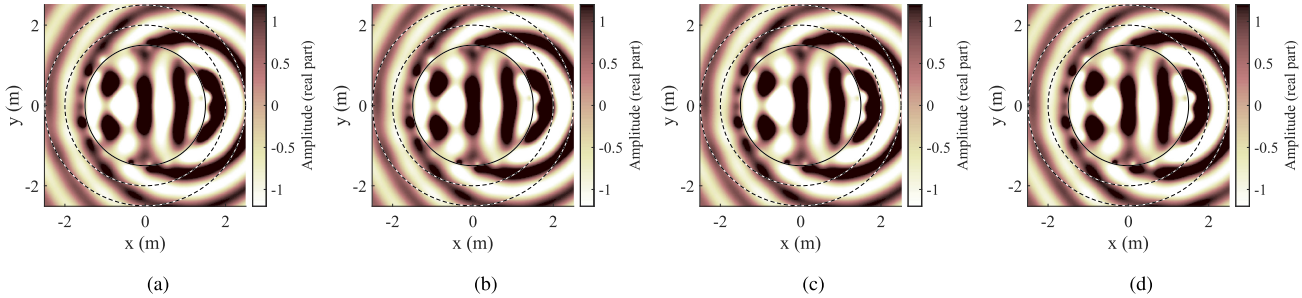


Fig. 10. Reproduced sound pressure distributions at 400 Hz when spherical wave from point source at $(1.0, 0, 0)$ m is reproduced by using spherical array of 144 cardioid sources oriented outward. (a) **Proposed (Uni)**; (b) **Proposed (Rad)**; (c) **MM**; (d) **PM**.

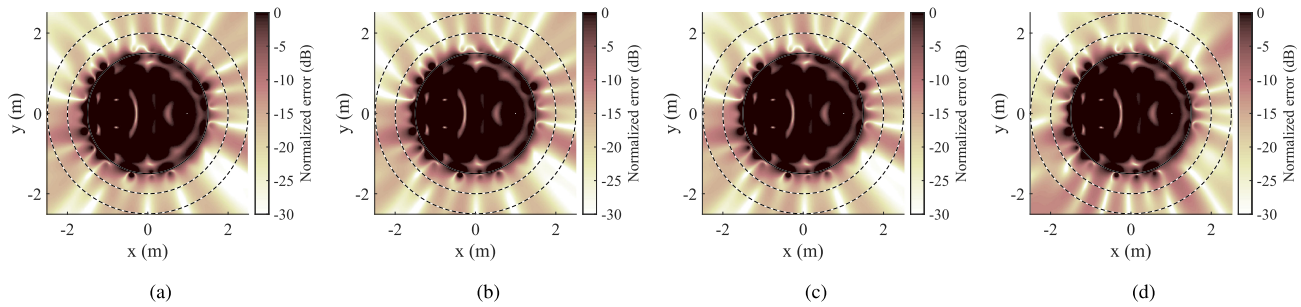


Fig. 11. Normalized error distributions at 400 Hz when spherical wave from point source at $(1.0, 0, 0)$ m is reproduced by using spherical array of 144 cardioid sources oriented outward. (a) **Proposed (Uni)**; (b) **Proposed (Rad)**; (c) **MM**; (d) **PM**.

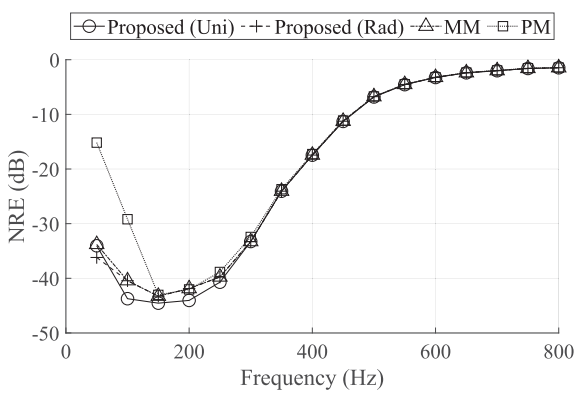


Fig. 12. Normalized reproduction error (NRE) plotted against frequency when spherical wave from point source at $(1.0, 0, 0)$ m is reproduced by using spherical array of 144 cardioid sources oriented outward.

monopole array was configured as follows. First, in the $xy$-plane, 64 monopole sources were aligned equidistantly on double squares centered at $(0, 0, 0)$ m with an inner side length of 3.0 m and an outer side length of 3.4 m. Then, five sets of these 64 monopole sources were aligned equidistantly along the $z$-direction at intervals of 0.5 m. Therefore, the total number of secondary sources was $L = 320$. The number of multizones was set as $Q = 2$, and the center and radius of $\Omega_{\rm int}^{(1)}$ and $\Omega_{\rm int}^{(2)}$ were $\boldsymbol{r}_{\rm c}^{(1)} = (0, 0.8, 0)$ m, $R_{\rm int}^{(1)} = 0.4$ m and $\boldsymbol{r}_{\rm c}^{(2)} = (0, -0.8, 0)$ m, $R_{\rm int}^{(2)} = 0.4$ m, respectively. The desired multizone sound fields were defined as $u_{\rm des}^{(1)}(\boldsymbol{r}) = a\exp({\rm j}kx)$ on $\Omega_{\rm int}^{(1)}$ with $a = 1$ and $u_{\rm des}^{(2)}(\boldsymbol{r}) = 0$ on $\Omega_{\rm int}^{(2)}$. In addition, exterior cancellation was attempted; therefore, the driving signals were obtained as

$$\hat{\boldsymbol{d}} = \left(\mathbf{A}_{\rm int}^{(1)} + \mathbf{A}_{\rm int}^{(2)} + \eta\mathbf{A}_{\rm ext} + \lambda\boldsymbol{I}_L\right)^{-1}\mathbf{b}_{\rm int}^{(1)}, \tag{76}$$

where $\mathbf{A}_{\rm int}^{(1)}$, $\mathbf{A}_{\rm int}^{(2)}$, and $\mathbf{b}_{\rm int}^{(1)}$ were calculated on the basis of the interior uniformly weighted $L_2$ norm and $\mathbf{A}_{\rm ext}$ was calculated on the basis of the exterior radiation-power norm. The truncation orders were set as $N_{\rm int}^{(1)} = \lceil (e/2)kR_{\rm int}^{(1)} \rceil$ for $\mathbf{A}_{\rm int}^{(1)}$ and $\mathbf{b}_{\rm int}^{(1)}$ and $N_{\rm int}^{(2)} = \lceil (e/2)kR_{\rm int}^{(2)} \rceil$ for $\mathbf{A}_{\rm int}^{(2)}$. The parameters $\eta$ and $\lambda$ were determined experimentally as $\eta = 10^{-2} \times \rho c k^2/2\pi$ and $\lambda = 10^{-3} \times \|\mathbf{A}_{\rm int}^{(1)} + \mathbf{A}_{\rm int}^{(2)} + \eta\mathbf{A}_{\rm ext}\|_2$.

Fig. 13 shows the reproduction results at 400 Hz. The black dots represent the positions of the monopole sources. Here, the normalized error distribution is calculated as $10\log_{10}|u_{\rm syn}(\boldsymbol{r}) - u_{\rm des}^{(1)}(\boldsymbol{r})|^2/|u_{\rm des}^{(1)}(\boldsymbol{r})|^2$ (dB) and the normalized power distribution is calculated as $10\log_{10}|u_{\rm syn}(\boldsymbol{r})|^2/|u_{\rm des}^{(1)}(\boldsymbol{r})|^2$ (dB). It can be seen that the normalized error is below $-30$ dB at almost all the points within $\Omega_{\rm int}^{(1)}$ and that the normalized power is below $-30$ dB at almost all the points within $\Omega_{\rm int}^{(2)}$ and outside the secondary sources.

In addition, to compare the performance of **Proposed** with **MM**, we also evaluate **MM** by using (21), (22), and (25) for $\mathbf{A}_{\rm int}^{(1)}$, $\mathbf{A}_{\rm int}^{(2)}$, $\mathbf{b}_{\rm int}^{(1)}$, and $\mathbf{A}_{\rm ext}$. In **MM**, the truncation order was set as $N_{\rm int} = \lceil \xi k R_{\rm int} \rceil$ and $N_{\rm ext} = \lceil \xi k R_{\rm ext} \rceil$, where $R_{\rm ext} =$

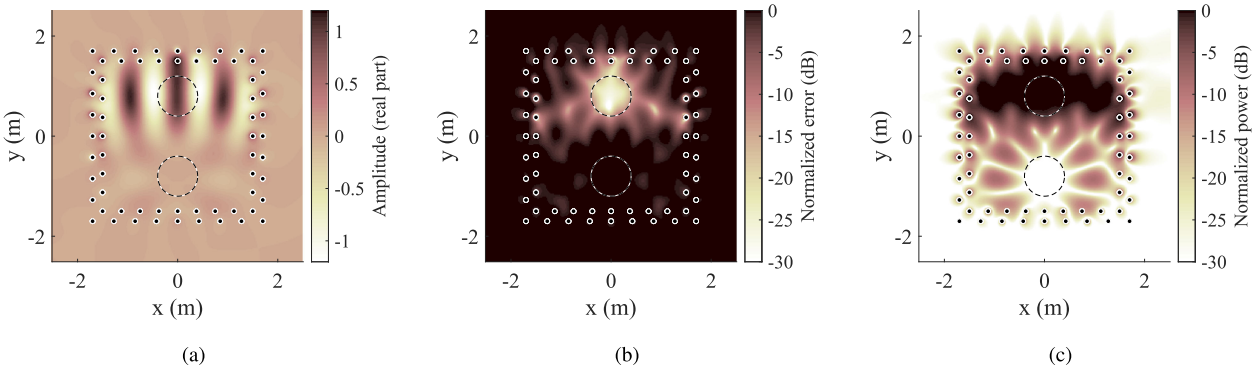


Fig. 13. Results of multizone reproduction with exterior cancellation at 400 Hz for **Proposed**. (a) Reproduced sound pressure distribution; (b) normalized error distribution; (c) normalized power distribution.

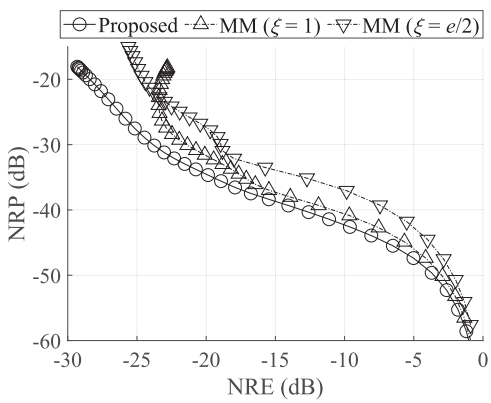


Fig. 14. Relationship between normalized reproduction error (NRE) and normalized radiation power (NRP) in multizone reproduction with exterior cancellation at 400 Hz.

$\max\{\|\boldsymbol{r}_l\|\}_{l=1}^{L} = 2.53$ m, and we investigated $\xi = 1$ and $\xi = e/2$ on the basis of the two rules of thumb. The regularization parameter in **MM** is determined in the same way as in **Proposed**, i.e., $\lambda = 10^{-3} \times \|\mathbf{A}_{\mathrm{int}}^{(1)} + \mathbf{A}_{\mathrm{int}}^{(2)} + \eta\mathbf{A}_{\mathrm{ext}}\|_2$.

The NRE and normalized radiation power (NRP) were used as evaluation criteria:

$$\mathrm{NRE} = 10\log_{10}\frac{\sum_{q=1}^{2}\int_{\Omega_{\mathrm{int}}^{(q)}}|u_{\mathrm{syn}}(\boldsymbol{r}) - u_{\mathrm{des}}^{(q)}(\boldsymbol{r})|^2\,\mathrm{d}\boldsymbol{r}}{\sum_{q=1}^{2}\int_{\Omega_{\mathrm{int}}^{(q)}}|u_{\mathrm{des}}^{(q)}(\boldsymbol{r})|^2\,\mathrm{d}\boldsymbol{r}}\ (\mathrm{dB}), \tag{77}$$

$$\mathrm{NRP} = 10\log_{10}\frac{\int_{\Omega'_{\mathrm{ext}}}|u_{\mathrm{syn}}(\boldsymbol{r})|^2\,\mathrm{d}\boldsymbol{r}}{\int_{\Omega'_{\mathrm{ext}}}|a|^2\,\mathrm{d}\boldsymbol{r}}\ (\mathrm{dB}), \tag{78}$$

where $\Omega'_{\mathrm{ext}}$ was set as the region between the inner sphere with a radius of 3.0 m and the outer sphere with a radius of 3.5 m that are both centered at $(0, 0, 0)$ m, and the spatial integrals were discretized with an interval of 0.05 m. Here, NRP is normalized by $a$ instead of $u_{\mathrm{des}}$ because $u_{\mathrm{des}}(\boldsymbol{r}) = 0$ in $\Omega_{\mathrm{ext}}$.

Since NRE and NRP have a trade-off relationship balanced by $\eta$, we investigated many different $\eta$ and plotted the relationship of NRE and NRP at 400 Hz in Fig. 14. Lower-left points indicate high reproduction accuracy with little radiation outside the secondary sources. It can be seen **Proposed** achieved lower NRE and NRP than **MM**.

## VI. Conclusion

We proposed a sound field reproduction method based on the spherical wavefunction expansion of sound fields. Instead of the empirical truncation in the current mode-matching method, the optimal weights on the expansion coefficients are derived analytically on the basis of the norm to be minimized in the proposed method. We also showed that the proposed method is easily applicable to multizone sound field reproduction and interior sound field reproduction with exterior cancellation. Numerical experiments confirmed that higher performance with lower computational cost can be achieved by the proposed method than by the mode-matching and pressure-matching methods.

## Appendix A
## Sufficient Condition of Interchangeability of Infinite Summation and Inner Product

In (36), the interchangeability of infinite summation and an inner product holds if the spherical wavefunction expansion of sound fields converges with respect to the norm $\|\cdot\|_{(*)}$. More particularly, the norm $\|\cdot\|_{(*)}$ has to satisfy the following condition:

$$\lim_{N\to\infty}\|\rho_N\|_{(*)} = 0, \tag{79}$$

where $\rho_N$ is the function defined as

$$\rho_N(\boldsymbol{r}) = u(\boldsymbol{r}) - \sum_{\nu,\mu}^{N}\mathring{u}_{\nu,\mu}^{\mathrm{int}}(\boldsymbol{r}_{\mathrm{c}})\varphi_{\nu,\mu}(\boldsymbol{r}-\boldsymbol{r}_{\mathrm{c}}) \tag{80}$$

for any interior sound field $u$ in interior sound field reproduction and

$$\rho_N(\boldsymbol{r}) = u(\boldsymbol{r}) - \sum_{\nu,\mu}^{N}\mathring{u}_{\nu,\mu}^{\mathrm{ext}}(\boldsymbol{r}_{\mathrm{c}})\psi_{\nu,\mu}(\boldsymbol{r}-\boldsymbol{r}_{\mathrm{c}}) \tag{81}$$

for any exterior sound field $u$ in exterior sound field reproduction. Here, we provide the proof. First, let $\tilde{u}_{1,N}$ and $\tilde{u}_{2,N}$ be

defined as

$$\tilde{u}_{1,N}(\boldsymbol{r}) = \sum_{\nu,\mu}^{N} \mathring{u}_{1,\nu,\mu}^{\mathrm{int}}(\boldsymbol{r}_{\mathrm{c}})\varphi_{\nu,\mu}(\boldsymbol{r}-\boldsymbol{r}_{\mathrm{c}}), \tag{82}$$

$$\tilde{u}_{2,N}(\boldsymbol{r}) = \sum_{\nu,\mu}^{N} \mathring{u}_{2,\nu,\mu}^{\mathrm{int}}(\boldsymbol{r}_{\mathrm{c}})\varphi_{\nu,\mu}(\boldsymbol{r}-\boldsymbol{r}_{\mathrm{c}}). \tag{83}$$

We also define $\rho_{1,N}$ and $\rho_{1,2}$ as $\rho_{1,N} = u_1 - \tilde{u}_{1,N}$ and $\rho_{2,N} = u_2 - \tilde{u}_{2,N}$, respectively. Then, since a finite summation and an inner product can be interchanged, $\langle u_1, u_2\rangle_{(*)}$ can be represented as the following form for any natural numbers $N_1$ and $N_2$:

$$\begin{aligned}\langle u_1, u_2\rangle_{(*)} &= \langle \tilde{u}_{1,N_1} + \rho_{1,N_1}, \tilde{u}_{2,N_2} + \rho_{1,N_2}\rangle_{(*)} \\ &= \langle \tilde{u}_{1,N_1}, \tilde{u}_{2,N_1}\rangle_{(*)} \\ &\quad + \langle \tilde{u}_{1,N_1}, \rho_{2,N_2}\rangle_{(*)} + \langle \rho_{1,N_2}, \tilde{u}_{2,N_2}\rangle_{(*)} \\ &\quad + \langle \rho_{1,N_2}, \rho_{2,N_2}\rangle_{(*)} \\ &= \sum_{\nu_1,\mu_1}^{N_1}\sum_{\nu_2,\mu_2}^{N_2} w_{\nu_1,\mu_1}^{\nu_2,\mu_2} \cdot \mathring{u}_{1,\nu_1,\mu_1}^{\mathrm{int}}(\boldsymbol{r}_{\mathrm{c}})^* \mathring{u}_{2,\nu_2,\mu_2}^{\mathrm{int}}(\boldsymbol{r}_{\mathrm{c}}) \\ &\quad + \langle u_1, \rho_{2,N_2}\rangle_{(*)} + \langle \rho_{1,N_1}, u_2\rangle_{(*)} \\ &\quad - \langle \rho_{1,N_1}, \rho_{2,N_2}\rangle_{(*)}.\end{aligned} \tag{84}$$

Here, the following inequality holds from the Cauchy-Schwarz inequality:

$$\begin{aligned}&\left|\langle u_1, \rho_{2,N_2}\rangle_{(*)} + \langle \rho_{1,N_1}, u_2\rangle_{(*)} - \langle \rho_{1,N_1}, \rho_{2,N_2}\rangle_{(*)}\right| \\ &\le \|u_1\|_{(*)}\|\rho_{2,N_2}\|_{(*)} + \|u_2\|_{(*)}\|\rho_{1,N_1}\|_{(*)} \\ &\quad + \|\rho_{1,N_1}\|_{(*)}\|\rho_{2,N_2}\|_{(*)}.\end{aligned} \tag{85}$$

From the conditions $\lim_{N\to\infty}\|\rho_{1,N}\|_{(*)} = 0$ and $\lim_{N\to\infty}\|\rho_{2,N}\|_{(*)} = 0$, the right-hand side of (85) converges to zeros as $N_1 \to \infty$ and $N_1 \to \infty$. Therefore, we obtain

$$\begin{aligned}\lim_{N_1\to\infty}\lim_{N_2\to\infty}\big(&\langle u_1, \rho_{2,N_2}\rangle_{(*)} + \langle \rho_{1,N_1}, u_2\rangle_{(*)} \\ &- \langle \rho_{1,N_1}, \rho_{2,N_2}\rangle_{(*)}\big) = 0.\end{aligned} \tag{86}$$

Then, (36) is proved by the following equality.

$$\begin{aligned}&\langle u_1, u_2\rangle_{(*)} - \sum_{\nu_1,\mu_1}\sum_{\nu_2,\mu_2} w_{\nu_1,\mu_1}^{\nu_2,\mu_2}\mathring{u}_{1,\nu_1,\mu_1}^{\mathrm{int}}(\boldsymbol{r}_{\mathrm{c}})^*\mathring{u}_{2,\nu_2,\mu_2}^{\mathrm{int}}(\boldsymbol{r}_{\mathrm{c}}) \\ &= \lim_{N_1\to\infty}\lim_{N_2\to\infty}\big(\langle u_1, \rho_{2,N_2}\rangle_{(*)} + \langle \rho_{1,N_1}, u_2\rangle_{(*)} \\ &\qquad - \langle \rho_{1,N_1}, \rho_{2,N_2}\rangle_{(*)}\big) \\ &= 0.\end{aligned} \tag{87}$$

## Appendix B
## Interior Weights in Case of Interior Uniformly Weighted $L_2$ Norm

First, the inner product corresponding to the norm $\|\cdot\|_{\mathrm{int,uni}}$ is given as

$$\langle u_1, u_2\rangle_{\mathrm{int,uni}} = \int_{\Omega_{\mathrm{int}}} u_1(\boldsymbol{r})^* u_2(\boldsymbol{r})\,\mathrm{d}\boldsymbol{r}. \tag{88}$$

Therefore, the interior weights $w_{\nu_1,\mu_1}^{\nu_2,\mu_2}$ are rewritten as

$$\begin{aligned}w_{\nu_1,\mu_1}^{\nu_2,\mu_2} &= \int_{\Omega_{\mathrm{int}}} \varphi_{\nu_1,\mu_1}(\boldsymbol{r}-\boldsymbol{r}_{\mathrm{c}})^*\varphi_{\nu_2,\mu_2}(\boldsymbol{r}-\boldsymbol{r}_{\mathrm{c}})\,\mathrm{d}\boldsymbol{r} \\ &= 4\pi\int_0^{R_{\mathrm{int}}} j_{\nu_1}(kr)^2 r^2\,\mathrm{d}r \\ &\quad \cdot \int_{\mathbb{S}^2} Y_{\nu_1,\mu_1}(\hat{\boldsymbol{r}})^* Y_{\nu_2,\mu_2}(\hat{\boldsymbol{r}})\,\mathrm{d}\hat{\boldsymbol{r}}.\end{aligned} \tag{89}$$

From the orthonormality of the spherical harmonics, one obtains

$$\int_{\mathbb{S}^2} Y_{\nu_1,\mu_1}(\hat{\boldsymbol{r}})^* Y_{\nu_2,\mu_2}(\hat{\boldsymbol{r}})\,\mathrm{d}\hat{\boldsymbol{r}} = \delta_{\nu_1,\nu_2}\delta_{\mu_1,\mu_2}. \tag{90}$$

In addition, from the identity [35]:

$$\frac{\mathrm{d}}{\mathrm{d}r}\left[\frac{r^3}{2}\left(j_\nu(kr)^2 - j_{\nu-1}(kr)j_{\nu+1}(kr)\right)\right] = j_\nu(kr)^2 r^2, \tag{91}$$

one obtains

$$\begin{aligned}&\int_0^{R_{\mathrm{int}}} j_\nu(kr)^2 r^2\,\mathrm{d}r \\ &= \frac{R_{\mathrm{int}}^3}{2}\left(j_\nu(kR_{\mathrm{int}})^2 - j_{\nu-1}(kR_{\mathrm{int}})j_{\nu+1}(kR_{\mathrm{int}})\right).\end{aligned} \tag{92}$$

Equations (90) and (92) yield (46).

## Appendix C
## Interior Weights in Case of Gaussian-Weighted $L_2$ Norm

The inner product corresponding to the norm $\|\cdot\|_{\mathrm{int,Gs}}$ is given as

$$\langle u_1, u_2\rangle_{\mathrm{int,Gs}} = \int_{\Omega_{\mathrm{int}}} \exp\left(-\frac{\|\boldsymbol{r}-\boldsymbol{r}_{\mathrm{c}}\|^2}{2\sigma^2}\right) u_1(\boldsymbol{r})^* u_2(\boldsymbol{r})\,\mathrm{d}\boldsymbol{r}. \tag{93}$$

Therefore, the interior weights $w_{\nu_1,\mu_1}^{\nu_2,\mu_2}$ are rewritten in a similar way to (89) as

$$w_{\nu_1,\mu_1}^{\nu_2,\mu_2} = \delta_{\nu_1,\nu_2}\delta_{\mu_1,\mu_2} 4\pi\int_0^{R_{\mathrm{int}}} \exp\left(-\frac{r^2}{2\sigma^2}\right) j_{\nu_1}(kr)^2 r^2\,\mathrm{d}r. \tag{94}$$

Therefore, (49) is yielded by the following equation:

$$\begin{aligned}&\frac{\mathrm{d}}{\mathrm{d}r}\left[\sum_{n=0}^{\infty}(-1)^n\frac{r^3}{2}\exp\left(-\frac{r^2}{4\sigma^2}\right) i_n\left(\frac{r^2}{4\sigma^2}\right)\right. \\ &\qquad \left.\cdot\left(j_{\nu-n}(kr)j_{\nu+n}(kr) - j_{\nu-n-1}(kr)j_{\nu+n+1}(kr)\right)\right] \\ &= \exp\left(-\frac{r^2}{2\sigma^2}\right) j_\nu(kr)^2 r^2.\end{aligned} \tag{95}$$

Next, we prove (95). First, let $a_{n,\nu}(r)$ be defined as

$$\begin{aligned}a_{n,\nu}(r) &= (-1)^n\frac{r^3}{2}\exp\left(-\frac{r^2}{4\sigma^2}\right) i_n\left(\frac{r^2}{4\sigma^2}\right) \\ &\quad \cdot\left(j_{\nu-n}(kr)j_{\nu+n}(kr) - j_{\nu-n-1}(kr)j_{\nu+n+1}(kr)\right).\end{aligned} \tag{96}$$

The derivative of $a_{n,\nu}(r)$ is written as

$$\begin{aligned}
&\frac{\mathrm{d}}{\mathrm{d}r}a_{n,\nu}(r)\\
&=(-1)^n r^2\exp\left(-\frac{r^2}{4\sigma^2}\right)\frac{r^2}{4\sigma^2}\\
&\quad\cdot\left\{\left[\frac{n+1}{r^2/(4\sigma^2)}i_n\left(\frac{r^2}{4\sigma^2}\right)-i_n\left(\frac{r^2}{4\sigma^2}\right)+i_n'\left(\frac{r^2}{4\sigma^2}\right)\right]\right.\\
&\qquad\cdot j_{\nu-n}(kr)j_{\nu+n}(kr)\\
&\qquad+\left[\frac{n}{r^2/(4\sigma^2)}i_n\left(\frac{r^2}{4\sigma^2}\right)+i_n\left(\frac{r^2}{4\sigma^2}\right)-i_n'\left(\frac{r^2}{4\sigma^2}\right)\right]\\
&\qquad\left.\cdot j_{\nu-n-1}(kr)j_{\nu+n+1}(kr)\right\}\\
&=(-1)^n r^2\exp\left(-\frac{r^2}{4\sigma^2}\right)\frac{r^2}{4\sigma^2}\\
&\quad\cdot\left\{\left[i_{n-1}\left(\frac{r^2}{4\sigma^2}\right)-i_n\left(\frac{r^2}{4\sigma^2}\right)\right]j_{\nu-n}(kr)j_{\nu+n}(kr)\right.\\
&\qquad\left.+\left[i_n\left(\frac{r^2}{4\sigma^2}\right)-i_{n+1}\left(\frac{r^2}{4\sigma^2}\right)\right]j_{\nu-n-1}(kr)j_{\nu+n+1}(kr)\right\}\\
&=b_{n,\nu}(r)-b_{n+1,\nu}(r),
\end{aligned}\tag{97}$$

where

$$\begin{aligned}
b_{n,\nu}(r)&=(-1)^n r^2\exp\left(-\frac{r^2}{4\sigma^2}\right)\frac{r^2}{4\sigma^2}\\
&\quad\cdot\left[i_{n-1}\left(\frac{r^2}{4\sigma^2}\right)-i_n\left(\frac{r^2}{4\sigma^2}\right)\right]j_{\nu-n}(kr)j_{\nu+n}(kr).
\end{aligned}\tag{98}$$

From the inequality:

$$|j_\nu(x)|\le|i_\nu(x)|\le\left(\frac{x}{2}\right)^\nu\frac{\sqrt{\pi}}{2\Gamma\left(\nu+\frac{3}{2}\right)}\exp\left(\frac{x^2}{4}\right),\tag{99}$$

one obtains the following relation in the sense of the compact convergence for $r\ge 0$:

$$\lim_{n\to\infty}b_{n,\nu}(r)=0.\tag{100}$$

Equation (99) can be shown from the series representation of the Bessel functions [23], [33]. Therefore, one obtains

$$\begin{aligned}
\frac{\mathrm{d}}{\mathrm{d}r}\sum_{n=0}^{\infty}a_{n,\nu}(r)&=\sum_{n=0}^{\infty}\frac{\mathrm{d}}{\mathrm{d}r}a_{n,\nu}(r)\\
&=b_{0,\nu}(r)\\
&=\exp\left(-\frac{r^2}{2\sigma^2}\right)j_\nu(kr)^2r^2.
\end{aligned}\tag{101}$$

This yields (95) and therefore (49).

## Appendix D
## Exterior Weights in Case of Exterior Uniformly Weighted $L_2$ Norm

The inner product corresponding to the norm $\|\cdot\|_{\mathrm{ext,uni}}$ is given as

$$\langle u_1,u_2\rangle_{\mathrm{ext,uni}}=\int_{\Omega'_{\mathrm{ext}}}u_1(\boldsymbol{r})^*u_2(\boldsymbol{r})\,\mathrm{d}\boldsymbol{r}.\tag{102}$$

Therefore, the exterior weights $v_{\nu_1,\mu_1}^{\nu_2,\mu_2}$ are rewritten as

$$v_{\nu_1,\mu_1}^{\nu_2,\mu_2}=\delta_{\nu_1,\nu_2}\delta_{\mu_1,\mu_2}4\pi\int_{R_{\mathrm{ext}}}^{R'_{\mathrm{ext}}}|h_{\nu_1}(kr)|^2r^2\,\mathrm{d}r.\tag{103}$$

From the identity:

$$\begin{aligned}
&\frac{\mathrm{d}}{\mathrm{d}r}\left[\frac{r^3}{2}\left(h_\nu(kr)^*h_\nu(kr)-h_{\nu-1}(kr)^*h_{\nu+1}(kr)\right)\right]\\
&\quad=h_\nu(kr)^*h_\nu(kr)r^2,
\end{aligned}\tag{104}$$

which can be derived similarly to (91), one obtains

$$\begin{aligned}
&\int_{R_{\mathrm{ext}}}^{R'_{\mathrm{ext}}}|h_\nu(kr)|^2r^2\,\mathrm{d}r\\
&=\frac{R'^3_{\mathrm{ext}}}{2}\left(|h_\nu(kR'_{\mathrm{ext}})|^2-h_{\nu-1}(kR'_{\mathrm{ext}})^*h_{\nu+1}(kR'_{\mathrm{ext}})\right)\\
&\quad-\frac{R^3_{\mathrm{ext}}}{2}\left(|h_\nu(kR_{\mathrm{ext}})|^2-h_{\nu-1}(kR_{\mathrm{ext}})^*h_{\nu+1}(kR_{\mathrm{ext}})\right).
\end{aligned}\tag{105}$$

This yields (54).

## Appendix E
## Exterior Weights in Case of Exterior Radiation-Power Norm

The inner product corresponding to the norm $\|\cdot\|_{\mathrm{ext,rad}}$ is given as

$$\begin{aligned}
&\langle u_1,u_2\rangle_{\mathrm{ext,rad}}\\
&=\frac{\mathrm{j}}{4\rho ck}\int_{S_{\mathrm{ext}}}\left[u_2(\boldsymbol{r})\frac{\partial}{\partial\hat{\boldsymbol{n}}(\boldsymbol{r})}u_1(\boldsymbol{r})^*-u_2(\boldsymbol{r})^*\frac{\partial}{\partial\hat{\boldsymbol{n}}(\boldsymbol{r})}u_1(\boldsymbol{r})\right]\mathrm{d}\boldsymbol{r}.
\end{aligned}\tag{106}$$

Therefore, the exterior weights $v_{\nu_1,\mu_1}^{\nu_2,\mu_2}$ are rewritten as

$$\begin{aligned}
v_{\nu_1,\mu_1}^{\nu_2,\mu_2}&=\delta_{\nu_1,\nu_2}\delta_{\mu_1,\mu_2}\frac{\pi\mathrm{j}R^2_{\mathrm{ext}}}{\rho c}\\
&\quad\cdot\left(h_{\nu_1}(kR_{\mathrm{ext}})h'_{\nu_1}(kR_{\mathrm{ext}})^*-h_{\nu_1}(kR_{\mathrm{ext}})^*h'_{\nu_1}(kR_{\mathrm{ext}})\right)\\
&=\delta_{\nu_1,\nu_2}\delta_{\mu_1,\mu_2}\frac{2\pi}{\rho ck^2},
\end{aligned}\tag{107}$$

where the second line is derived using the Wronskian of the spherical Hankel functions [33]. This yields (57).

Next, we give the proof of (62) and (63). As shown in [24], the following two identities hold for $T_{\nu_1,\mu_1}^{\nu_2,\mu_2}(\cdot)$:

$$T_{\nu_1,\mu_1}^{\nu_2,\mu_2}(-\boldsymbol{r})=T_{\nu_2,\mu_2}^{\nu_1,\mu_1}(\boldsymbol{r})^*,\tag{108}$$

$$T_{\nu_1,\mu_1}^{\nu_2,\mu_2}(\boldsymbol{r}+\boldsymbol{r}')=\sum_{\nu,\mu}T_{\nu_1,\mu_1}^{\nu,\mu}(\boldsymbol{r})T_{\nu,\mu}^{\nu_2,\mu_2}(\boldsymbol{r}').\tag{109}$$

Therefore, one obtains

$$
\begin{aligned}
(\mathbf{A})_{l_1,l_2} &= \frac{2\pi}{\rho c k^2} \sum_{\nu,\mu} \mathring{g}^{\text{ext}}_{l_1,\nu,\mu}(\boldsymbol{r}_{l_1})^* \mathring{g}^{\text{ext}}_{l_2,\nu,\mu}(\boldsymbol{r}_{l_2}) \\
&= \frac{2\pi}{\rho c k^2} \sum_{\nu,\mu} \left( \sum_{\nu_1,\mu_1}^{N_{l_1}} T^{\nu_1,\mu_1}_{\nu,\mu}(\boldsymbol{r}_{\text{c}} - \boldsymbol{r}_{l_1}) \beta_{l_1,\nu_1,\mu_1} \right)^* \\
&\quad \cdot \left( \sum_{\nu_2,\mu_2}^{N_{l_2}} T^{\nu_2,\mu_2}_{\nu,\mu}(\boldsymbol{r}_{\text{c}} - \boldsymbol{r}_{l_2}) \beta_{l_2,\nu_2,\mu_2} \right) \\
&= \frac{2\pi}{\rho c k^2} \sum_{\nu_1,\mu_1}^{N_{l_1}} \sum_{\nu_2,\mu_2}^{N_{l_2}} \beta^*_{l_1,\nu_1,\mu_1} \beta_{l_2,\nu_2,\mu_2} \\
&\quad \sum_{\nu,\mu} T^{\nu_1,\mu_1}_{\nu,\mu}(\boldsymbol{r}_{\text{c}} - \boldsymbol{r}_{l_1})^* T^{\nu_2,\mu_2}_{\nu,\mu}(\boldsymbol{r}_{\text{c}} - \boldsymbol{r}_{l_2}) \\
&= \frac{2\pi}{\rho c k^2} \sum_{\nu_1,\mu_1}^{N_{l_1}} \sum_{\nu_2,\mu_2}^{N_{l_2}} \beta^*_{l_1,\nu_1,\mu_1} \beta_{l_2,\nu_2,\mu_2} T^{\nu_2,\mu_2}_{\nu,\mu}(\boldsymbol{r}_{l_2} - \boldsymbol{r}_{l_2}).
\end{aligned} \tag{110}
$$

This yields (62). Similarly, (63) can be obtained.

## References


[1] A. J. Berkhout, D. De Vries, and P. Vogel, "Acoustic control by wave field synthesis," *J. Acoust. Soc. America*, vol. 93, no. 5, pp. 2764–2778, 1993.

[2] S. Spors, R. Rabenstein, and J. Ahrens, "The theory of wave field synthesis revisited," in *Proc. 124th AES Conv.*, Amsterdam, The Netherlands, Oct. 2008.

[3] M. A. Poletti, "Three-dimensional surround sound systems based on spherical harmonics," *J. Audio Eng. Soc.*, vol. 53, no. 11, pp. 1004–1025, 2005.

[4] J. Ahrens and S. Spors, "Analytical driving functions for higher order ambisonics," in *Proc. IEEE Int. Conf. Acoust., Speech, Signal Process.*, Las Vegas, NV, USA, Mar. 2008, pp. 373–376.

[5] M. A. Poletti and T. D. Abhayapala, "Interior and exterior sound field control using general two-dimensional first-order sources," *J. Acoust. Soc. America*, vol. 129, no. 1, pp. 234–244, 2011.

[6] J. Ahrens and S. Spors, "An analytical approach to sound field reproduction using circular and spherical loudspeaker distributions," *Acta Acustica United Acustica*, vol. 94, pp. 988–999, 2008.

[7] F. Winter, J. Ahrens, and S. Spors, "On analytic methods for 2.5-D local sound field synthesis using circular distributions of secondary sources," *IEEE Trans. Audio, Speech, Lang. Process.*, vol. 24, no. 5, pp. 914–926, May 2016.

[8] S. Koyama, K. Furuya, Y. Hiwasaki, and Y. Haneda, "Analytical approach to wave field reconstruction filtering in spatio-temporal frequency domain," *IEEE Trans. Audio, Speech, Lang. Process.*, vol. 21, no. 4, pp. 685–696, Apr. 2013.

[9] S. Koyama, K. Furuya, Y. Hiwasaki, Y. Haneda, and Y. Suzuki, "Wave field reconstruction filtering in cylindrical harmonic domain for with-height recording and reproduction," *IEEE/ACM Trans. Audio, Speech, Lang. Process.*, vol. 22, no. 10, pp. 1546–1557, Oct. 2014.

[10] O. Kirkeby and P. A. Nelson, "Reproduction of plane wave sound fields," *J. Acoust. Soc. America*, vol. 94, no. 5, pp. 2992–3000, 1993.

[11] P. A. Nelson, "Active control of acoustic fields and the reproduction of sound," *J. Sound Vib.*, vol. 177, no. 4, pp. 447–477, 1993.

[12] P.-A. Gauthier and A. Berry, "Sound-field reproduction in-room using optimal control techniques: Simulations in the frequency domain," *J. Acoust. Soc. America*, vol. 117, no. 2, pp. 662–678, 2005.

[13] P. N. Samarasinghe, M. A. Poletti, S. M. A. Salehin, T. D. Abhayapala, and F. M. Fazi, "3D soundfield reproduction using higher order loudspeakers," in *Proc. IEEE Int. Conf. Acoust., Speech, Signal Process.*, Vancouver, BC, Canada, May 2013, pp. 306–310.

[14] M. A. Poletti, F. M. Fazi, and P. A. Nelson, "Sound-field reproduction systems using fixed-directivity loudspeakers," *J. Acoust. Soc. America*, vol. 127, no. 6, pp. 3590–3601, 2010.

[15] T. Betlehem and T. D. Abhayapala, "Theory and design of sound field reproduction in reverberant rooms," *J. Acoust. Soc. America*, vol. 117, no. 4, pp. 2100–2111, 2005.

[16] J. Daniel, "Spatial sound encoding including near field effect: Introducing distance coding filters and a viable, new ambisonics format," in *Proc. 23rd AES Int. Conf.*, Copenhagen, Denmark, May 2003, Paper 16.

[17] N. Ueno, S. Koyama, and H. Saruwatari, "Listening-area-informed sound field reproduction based on circular harmonic expansion," in *Proc. IEEE Int. Conf. Acoust., Speech, Signal Process.*, New Orleans, LA, USA, Mar. 2017, pp. 111–115.

[18] N. Ueno, S. Koyama, and H. Saruwatari, "Listening-area-informed sound field reproduction with Gaussian prior based on circular harmonic expansion," in *Proc. Joint Workshop Hands-free Speech Commun. Microphone Arrays*, San Francisco, CA, USA, Mar. 2017, pp. 196–200.

[19] N. Ueno, S. Koyama, and H. Saruwatari, "Sound field reproduction with exterior radiation cancellation using analytical weighting of harmonic coefficients," in *Proc. IEEE Int. Conf. Acoust., Speech, Signal Process.*, Calgary, AB, Canada, Apr. 2018, pp. 466–470.

[20] W. Jin and W. B. Kleijn, "Multizone soundfield reproduction in reverberant rooms using compressed sensing techniques," in *Proc. IEEE Int. Conf. Acoust., Speech, Signal Process.*, Florence, Italy, May 2014, pp. 4728–4732.

[21] Y. J. Wu and T. D. Abhayapala, "Spatial multizone soundfield reproduction: Theory and design," *IEEE Trans. Audio, Speech, Lang. Process.*, vol. 19, no. 6, pp. 1711–1720, Aug. 2011.

[22] J.-W. Choi and Y.-H. Kim, "Generation of an acoustically bright zone with an illuminated region using multiple sources," *J. Acoust. Soc. America*, vol. 111, no. 4, pp. 1695–1700, 2002.

[23] A. Kirsch and F. Hettlich, *The Mathematical Theory of Time-Harmonic Maxwell's Equations*. Cham, Switzerland: Springer, 2015.

[24] P. A. Martin, *Multiple Scattering: Interaction of Time-Harmonic Waves with N Obstacles*. New York, NY, USA: Cambridge Univ. Press, 2006.

[25] J. Meyer and G. Elko, "A highly scalable spherical microphone array based on an orthogonal decomposition of the soundfield," in *Proc. IEEE Int. Conf. Acoust., Speech, Signal Process.*, Orlando, FL, USA, May 2002, pp. II–1781–1784.

[26] T. D. Abhayapala and D. B. Ward, "Theory and design of high order sound field microphones using spherical microphone array," in *Proc. IEEE Int. Conf. Acoust., Speech, Signal Process.*, Orlando, FL, USA, May 2002, pp. II–1949–1952.

[27] A. Laborie, R. Bruno, and S. Montoya, "A new comprehensive approach of surround sound recording," in *Proc. 114th AES Conv.*, Amsterdam, The Netherlands, Oct. 2003.

[28] B. Rafaely, *Fundamentals of Spherical Array Processing*. Berlin, Germany: Springer, 2015.

[29] P. N. Samarasinghe, T. D. Abhayapala, and M. A. Poletti, "3D spatial soundfield recording over large regions," in *Proc. Int. Workshop Acoust. Signal Enhancement*, Aachen, Germany, Sep. 2012, pp. 1–4.

[30] P. N. Samarasinghe, T. D. Abhayapala, and M. A. Poletti, "Wavefield analysis over large areas using distributed higher order microphones," *IEEE/ACM Trans. Audio, Speech, Lang. Process.*, vol. 22, no. 3, pp. 647–658, Mar. 2014.

[31] N. Ueno, S. Koyama, and H. Saruwatari, "Sound field recording using distributed microphones based on harmonic analysis of infinite order," *IEEE Signal Process. Lett.*, vol. 25, no. 1, pp. 135–139, Jan. 2018.

[32] F. Zotter, "Analysis and synthesis of sound-radiation with spherical arrays," Ph.D. dissertation, University of Music and Performing Arts, Graz, Austria, 2009.

[33] E. G. Williams, *Fourier Acoustics: Sound Radiation and Nearfield Acoustical Holography*. London, U.K.: Academic Press, 1999.

[34] X. Chen and R. Womerlsy. Spherical t-design with d = (t + 1)^2 points. (Accessed on Oct. 26, 2018). [Online]. Available: http://www.polyu.edu.hk/ama/staff/xjchen/sphdesigns.html

[35] C. A. Anderson, P. D. Teal, and M. A. Poletti, "Spatial correlation of radial Gaussian and uniform spherical volume near-field source distributions," *IEEE/ACM Trans. Audio, Speech, Lang. Process.*, vol. 24, no. 1, pp. 143–150, Jan. 2016.

**Natsuki Ueno** (S'17) received the B.E. degree in engineering from Kyoto University, Kyoto, Japan, in 2016, and the M.S. degree in information science and technology from the University of Tokyo, Tokyo, Japan, in 2018. He is currently working toward the Ph.D. degree at Graduate School of Information Science and Technology, the University of Tokyo, Tokyo, Japan. His research interest includes spatial audio and acoustic signal processing.

**Shoichi Koyama** (M'10) received the B.E., the M.S., and the Ph.D. degrees from the University of Tokyo, Tokyo, Japan, in 2007, 2009, and 2014, respectively. In 2009, he was a Researcher in acoustic signal processing with the Nippon Telegraph and Telephone Corporation. He moved to the University of Tokyo in 2014, and since 2018, he has been an Assistant Professor (Lecturer) there. From 2016 to 2018, he was also a Visiting Researcher and JSPS overseas Research Fellow with Paris Diderot University (Paris7), Institut Langevin, Paris, France. His research interests include acoustic inverse problems, sound field analysis and synthesis, and spatial audio. Dr. Koyama is a member of the Acoustical Society of America, the Audio Engineering Society, the Institute of Electronics, Information and Communication Engineers, and the Acoustical Society of Japan (ASJ). He was the recipient of Itakura Prize Innovative Young Researcher Award by ASJ in 2015, and the Research Award by Funai Foundation for Information Technology in 2018.

**Hiroshi Saruwatari** (M'00) received the B.E., the M.E., and the Ph.D. degrees from Nagoya University, Nagoya, Japan, in 1991, 1993, and 2000, respectively. He joined SECOM IS Laboratory, Japan, in 1993, and Nara Institute of Science and Technology, Japan, in 2000. From 2014, he has been a Professor with The University of Tokyo, Tokyo, Japan. His research interests include statistical audio signal processing, blind source separation (BSS), and speech enhancement. Dr. Saruwatari was the recipient of paper awards from IEICE in 2001 and 2006, from TAF in 2004, 2009, 2012, and 2018, from IEEE-IROS2005 in 2006, and from APSIPA in 2013 and 2018. He was also the recipient of DOCOMO Mobile Science Award in 2011, Ichimura Award in 2013, The Commendation for Science and Technology by the Minister of Education in 2015, Achievement Award from IEICE in 2017, and Hoko-Award in 2018. He has been professionally involved in various volunteer works for IEEE, EURASIP, IEICE, and ASJ. He is an APSIPA Distinguished Lecturer from 2018.